6-2020

Simulation of Cu Precipitation in Fe-Cu Dilute Alloys with Cluster Mobility

Senlin Cui
University of Wisconsin-Madison

Mahmood Mamivand
Boise State University

Dane Morgan
University of Wisconsin-Madison

Publication Information

Cui, Senlin; Mamivand, Mahmood; and Morgan, Dane. (2020). "Simulation of Cu Precipitation in Fe-Cu Dilute Alloys with Cluster Mobility". *Materials & Design, 191*, 108574-1 - 108574-14. https://dx.doi.org/10.1016/j.matdes.2020.108574

Materials and Design 191 (2020) 108574

Contents lists available at ScienceDirect

Materials and Design

journal homepage: www.elsevier.com/locate/matdes

Simulation of Cu precipitation in Fe-Cu dilute alloys with cluster mobility

Senlin Cui [a,*], Mahmood Mamivand [b], Dane Morgan [a,*]

[a] Department of Materials Science and Engineering, University of Wisconsin-Madison, 1509 University Ave, Madison, WI 53706, USA
[b] Department of Mechanical and Biomedical Engineering, Boise State University, Boise, ID 83725, USA

HIGHLIGHTS

- Extension of Slezov et al.'s cluster dynamics theory with cluster mobility
- Effects of model parameters of the new model on precipitation kinetics
- Accurate modeling of the Cu precipitation in Fe-Cu dilute alloys
- Discussion of impurity effects on Cu precipitation kinetics

GRAPHICAL ABSTRACT

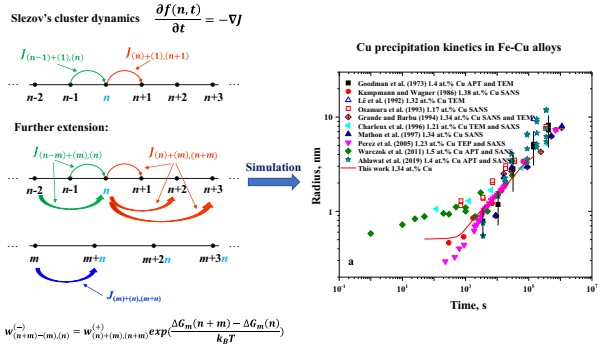

ARTICLE INFO

Article history:
Received 3 December 2019
Received in revised form 27 January 2020
Accepted 17 February 2020
Available online 19 February 2020

Keywords:
Cu-rich precipitates
Fe-Cu dilute alloys
Cluster dynamics
Coagulation
Reactor pressure vessel steels

ABSTRACT

Cu-rich precipitates formation is associated with the precipitation hardening of Fe-Cu based steels and the embrittlement of reactor pressure vessel steels under neutron irradiation. The accurate modeling of the time evolution of Cu-rich precipitates is therefore of fundamental importance for the design of Fe-Cu based steels and the prediction of the irradiation induced shift of the ductile to brittle transition temperature of reactor pressure vessels. This work applies cluster dynamics with mobile Cu monomers and clusters to model Cu precipitation in dilute Fe-Cu alloys at several temperatures. Optimized model parameters can be used to simulate the mean radius, number density, volume fraction, and matrix composition evolution during isothermal annealing with reasonable accuracy. The possible reduction of the mobility of Cu-rich clusters due to additional alloying elements in Fe-Cu based steels is discussed.

1. Introduction

Precipitation of Cu-rich phases has important effects on the mechanical properties of Fe-Cu based steels. Cu addition is known to strengthen structural steels due to the precipitation of Cu clusters after thermal heat treatment [1–3], and thus Cu containing steels can provide combined high strength, good impact toughness, promising weldability, and corrosion resistance [2,3]. However, residue amount of Cu (about 0.1 at.%) in reactor pressure vessel (RPV) steels induces the formation of fine scale Cu-rich precipitates (CRPs) under neutron irradiation which causes an undesirable radiation embrittlement of RPVs [4–6]. The understanding of the mechanisms and kinetics of Cu precipitation in Fe-Cu based steels under both thermal aging and irradiation is, therefore, of fundamental importance in the further advancements of various technological applications.

Developing physical model to predict the precipitation kinetics of CRPs and further the mechanical properties of Fe-Cu based steels is one of the key approaches to gain insight into the role of Cu in Fe-Cu based steels. A fundamental step is to develop precipitation model for

* Corresponding authors.
E-mail addresses: cuisenlin@gmail.com (S. Cui), ddmorgan@wisc.edu (D. Morgan).

https://doi.org/10.1016/j.matdes.2020.108574

Cu in dilute body centred cubic (bcc) Fe solution, and as a representative problem for precipitation modeling, there are many previously developed mesoscale models for Cu precipitates evolution in bcc Fe. More specifically, previous mesoscale approaches include the modified Langer and Schwartz (MLS) method [7], the Kampmann and Wagner numerical (KWN) model [8,9], the cluster dynamics (CD) models [10–18], and other precipitation models [19–21].

However, most of these simulation works [7,8,10,12,14,16,17,19–21] cannot accurately and simultaneously model the time evolution of all the precipitation properties including number density, matrix composition, mean radius, as well as volume fraction. This issue stems from the nature of Cu precipitation kinetics in bcc Fe. Instead of forming the so-called "growth region" with the rate law of $\overline{R} \propto t^{\frac{1}{2}}$, the experimentally measured mean radius of Cu precipitates follows the $\overline{R} \propto t^{\frac{1}{3}}$ growth law starting at the very early aging stage [8,22]. This feature agrees with the growth law of the "coarsening region" as predicted by the Lifshitz-Slyozov-Wagner (LSW) theory [23,24]. In fact, to mitigate the difference between the model-predicted and measured mean radius of Cu precipitates, large values of Cu diffusivity (typically 10^{-18} to 10^{-19} m^2/s at 500 °C, which is about 10^2 to 10^3 times larger than the expected value according to experiments) were used to shift the predicted coarsening region to an earlier time to match the experimental data [7,10,12,14,18–20]. Even with this unreasonable Cu diffusivity, these modeling works still generally predicted lower coarsening rates than experiments and/or erroneous volume fraction of Cu precipitates at the early aging stage.

Recent kinetic Monte Carlo (kMC) simulations by Soisson and Fu [25] indicated that lacking the physics of Cu cluster mobility is a likely source of the issues seen in many models of Cu precipitation. Jourdan et al. [15] demonstrated that the CD theory with mobility of Cu clusters can model the kinetics of CRPs formation in Fe-Cu alloys with an example alloy Fe-1.34 at.% Cu at 500 °C. Even though the agreement to the experimental precipitation kinetics was substantially improved, their model parameters were only fitted to the kMC results as derived by Soisson and Fu [25] and comparison to additional experimental data sets would be useful to demonstrate that all the physics is really in the model. In a more detailed work, Stechauner and Kozeschnik [9] took into account the physics of particle coalescence and showed an accurate modeling of Cu precipitation in bcc Fe, however, they used the KWN model. Although the KWN model has much higher computational efficiency compared to CD, it used the classical nucleation theory, and therefore only clusters larger than the critical nucleus are considered, and a quasi-equilibrium particle size distribution is assumed at the outset, and the detailed information of each sized clusters are not precisely tracked. In addition, multiple kMC [25–31] studies had been done for Cu cluster mobility in dilute Fe-Cu alloys, but the kMC method has many computational challenges in treating large length and time scales.

Due to the advantage in efficient and highly flexible modeling of large time scale evolution of complex clusters and point defects in materials, the CD model was extensively utilized to study the precipitation of Cu in bcc Fe under both thermal aging and irradiation aimed to understand the precipitation kinetics of CRPs in RPV steels and other Fe-Cu based alloys [10–18]. However, only limited experimental data sets were utilized in these modeling works. There is little evidence that the calibrated model parameters are representative in a wide enough composition and temperature range or at the service condition of RPV steels. It should be noted that the version of CD model used by Jourdan et al. [15] is different from that of Slezov et al. [32,33] which is widely used particularly for multicomponent stoichiometric phase precipitation modeling. However, the CD theory of Slezov et al. [32,33] is only limited to monomers with mobility, thus further development of the CD theory to include the physics of cluster mobility is required for the purpose of multicomponent precipitation modeling in Fe-Cu based alloys. It should be noted that the recent work by Liu et al. [34] combined the Slezov's CD model with Jourdan et al.'s definition of fluxes for mobile clusters to model cluster evolution with cluster mobility in ion-irradiated 3C-SiC materials. However, the paper offered few details about the model and did not provide their derivation or the resulting equations, made it unable to serve as a foundation for the modeling of mobile clusters in the Slezov's CD formalism.

Therefore, the goal of the present article is to develop a new CD model for Cu evolution in bcc Fe to handle the above discussed issues. To be specific, the model will (i) include the physics of mobile Cu clusters, which has been demonstrated to play a critical role in Cu cluster evolution, (ii) be built within the widely adopted CD framework of Slezov et al. [32,33], (iii) be explored phenomenologically to support a better understanding of the roles of key parameters, (iv) be fitted to and validated against multiple data sets to help assure the accuracy of the fitted values and the model robustness.

This paper is arranged as follows. Section 2 describes the generalization of the Slezov model to include cluster mobility. Section 3 describes the modeling work, including the simulation methods (Section 3.1), the specific parameters determined for the modified CD model (Section 3.2), the results of a phenomenological study of how the key CD model parameters impacting the cluster evolution (Section 3.3), and the results and discussions of the detailed comparisons of the model predictions to the experimental data (Section 3.4). Section 4 provides a general discussion of what this modeling effort teaches us about Cu and CRPs in Fe-Cu alloys and Section 5 gives a final summary and conclusions.

2. Extension of the CD model with cluster mobility

The CD theory was originally developed by Farkas et al. [35–39] to treat the nucleation kinetics of water from vapor without considering coalescence and splitting and including just single molecular H_2O motion (i.e., no cluster mobility). Even for CD models without cluster mobility, coalescence, and splitting, there are different versions available in the literature, which depend on the detailed form of the absorption and emission coefficients. CD models have also been extended along two key directions, to treat multi-component (species) and to treat mobile clusters, coalescence, and splitting. With respect to multi-component (species), the CD theory was further developed by Slezov et al. [32,33] to model single and multi-component (species) stoichiometric compound precipitation. Another version of CD model was presented in a review paper by Clouet et al. [40], which can be used to model precipitation for single component (species) phases. With respect to mobile clusters, coalescence, and splitting, Binder et al. [40,41] generalized the nucleation theory to consider cluster coalescence and splitting mechanisms. Jourdan et al. [15] then extended Clouet et al.'s CD model to study the Cu precipitation in Fe-1.34 at.% Cu alloys with the effects of mobile clusters and their coalescence included. It is worth noting that a new continuity equation was proposed by Jourdan et al. [15] to account for clusters up to a size n_{max} being mobile through diffusion. Although written somewhat differently, the equation is mathematically equivalent to that presented by Clouet et al. [40]. From this brief summary it is clear that the extensions of CD to multi-component (species) and to mobile clusters, coalescence, and splitting have taken separate paths and there is presently no clearly derived and articulated CD framework which includes them both. Therefore, in the present work, we utilize the CD theory in the framework of Slezov et al. [32,33] and extend the theory to include mobile clusters, coalescence, and splitting. We start from a brief introduction of the CD theory from Slezov et al. [32,33], and then include the new developments.

Assume the nucleation and growth of clusters happen by aggregation or emission of single mobile particles in a dynamic equilibrium. The flux (J) of clusters with size of n to clusters with size of $n+1$ in a single component precipitate phase can be written as [32,33]:

$$J_{(n)+(1),(n+1)} = w^{(+)}_{(n)+(1),(n+1)} f(n,t) - w^{(-)}_{(n+1)-(1),(n)} f(n+1,t) \quad (1)$$

where the coefficient $w^{(+)}_{(n)+(1),(n+1)}$ is the rate of clusters with size of n that absorb single particles (atoms) to form clusters with size of $n+1$, $w^{(-)}_{(n+1)-(1),(n)}$ is the rate of clusters with size of $n+1$ emit single particles to degrade to clusters with size of n, and $f(n,t)$ is the distribution function of clusters with size of n, containing n single particles, at time t. $f(n,t)$ has the implication of temporal concentration of clusters of size n and can be treated as the number of clusters of size n per unit volume at time t. The absorption coefficient equals the rate of surface mobile particles of the considered component reaching the precipitate/matrix interface in one step of motion. The surface concentration of mobile particles is derived by the continuity of the surface diffusion flux and bulk diffusion flux. Considering spherical precipitates, the absorption coefficient is given as [32]:

$$w^{(+)}_{(n)+(1),(n+1)} = 4\pi R^2 \frac{D^*_1}{\alpha_{1\beta}} c_{1\beta} \left\{ \frac{1}{1+\left[\left(\frac{D^*_1}{D_{(1)}}\right)\left(\frac{R}{\alpha_{1\beta}}\right)\right]} \right\} \tag{2}$$

where $R = R_n + R_1$ is the capture radius with R_i the radius of clusters of size i (in Slezov et al.'s original derivation $R = R_n$ was used and the contribution of R_1 was assumed to be negligible), D^*_1 is the partial diffusion coefficient of single particles near the precipitate/matrix interface (note that this quantity does not enter the final model for diffusion-limited precipitate growth), $\alpha_{1\beta}$ is the radius of single particles in the matrix phase or the characteristic length scale, $c_{1\beta}$ is the volume concentration of single particles in the matrix phase, and $D_{(1)}$ is the partial diffusivity of single particles in the bulk. Note that in the present work the partial diffusivity is taken to be the intrinsic diffusivity, which is approximately equal to the related tracer diffusivity times thermodynamic factor $\varnothing$. $\varnothing$ is typically close to 1 for a dilute solution [42,43], so tracer diffusivity will be used in this work. Furthermore, impurity diffusivities are the limiting values of tracer diffusivities of solutes in dilute alloys, so it will in fact be impurity diffusivities that are used as diffusivities of solutes throughout this paper.

For diffusion-limited growth of precipitates ($1 \ll \left[\left(\frac{D^*_1}{D_{(1)}}\right)\left(\frac{R}{\alpha_{1\beta}}\right)\right]$) [32],

$$w^{(+)}_{(n)+(1),(n+1)} \approx 4\pi R D_{(1)} c_{1\beta} \tag{3}$$

At the initial state, $c_{1\beta} = \frac{x_{1\beta}}{\Omega}$, when the number of particles per unit volume is used as concentration. $x_{1\beta}$ is the mole fraction of single particles in the matrix phase, and Ω is the averaged volume of single particles in the matrix.

The relationship between emission coefficient and absorption coefficient has been derived from equilibrium or constraint equilibrium cluster size distributions and applying detailed balance to thermodynamic nonequilibrium states (the traditional approach) [44,45], or internal equilibrium assumption of both matrix and precipitate phases (local equilibrium assumption) and the concepts of virtual and real states of the matrix phase [32], both yielding equivalent results. According to Slezov et al. [32,33], $w^{(-)}_{(n+1)-(1),(n)} = w^{(+)}_{(n)+(1),(n+1)} \exp\left(\frac{\Delta g}{k_B T}\right)$ and Δg is the total change of the Gibbs free energy in the transfer of a considered particle from the virtual state to the real state, k_B is the Boltzmann constant, and T is temperature in Kelvin. Although Selzov et al.'s virtual state based derivation [32,33] is more rigorous, here we avoid the introduction of the virtual state and the real state concepts for simplicity and the traditional approach is used, since both derivations lead to the same conclusion. According to detailed balance, the flux in Eq. (1) at equilibrium condition is 0 ($J_{(n)+(1),(n+1)}{}^{eq} = 0$), from which one can derive the relationship between emission coefficient and absorption coefficient as [32]:

$$w^{(-)}_{(n+1)-(1),(n)} = w^{(+)}_{(n)+(1),(n+1)} \exp\left(\frac{\Delta G(n+1) - \Delta G(n)}{k_B T}\right) \tag{4}$$

where $\Delta G(n)$ is the Gibbs energy of formation of α phase clusters of size n ($n > 1$) from the matrix phase β with the state of single particles in the matrix phase or monomers as reference state, and $\Delta G(n)$ is given as:

$$\Delta G(n) = n\left(\mu^q_1 - \mu^\beta_1\right) + \sigma A(n) \tag{5}$$

where μ^p_1 is the chemical potential of single particles in the ambient p phase, σ is the interfacial energy per unit area (can be also cluster size dependent), and $A(n) = 4\pi {R_n}^2$ is the surface area of clusters with size n. It should be noted that Eq. (5) does not consider the pressure difference between the matrix and clusters due to lattice strain, since coherent precipitates are formed with little lattice mismatch in the present paper. Otherwise, a pressure term may need to be considered.

If both the matrix and precipitate phases are multicomponent, the above discussed equations can be applied approximately by defining structural units having the same composition as the clusters and with a total of one particle included. With this generalization the absorption coefficient is defined as $w^{(+)}_{(n)+(1),(n+1)} \approx 4\pi R_n {D_{(1)}}^{eff} c_\beta$, where ${D_{(1)}}^{eff}$ is the effective diffusivity and c_β is the total volume concentration of the matrix phase. The effective diffusivity is given by $\left(\sum_{i=1}^{k} \frac{{v_{i\alpha}}^2}{x_{i\beta} D^i_{(1)}}\right)^{-1}$ with $v_{i\alpha}$, $x_{i\beta}$, and $D^i_{(1)}$ are the stoichiometric coefficient of component i in the precipitate phase, mole fraction of i in the matrix phase, and partial diffusivity of component i in the matrix phase, respectively. Here $v_{i\alpha} \le 1$ is presumed. The formation energy of clusters with size n ($n > 1$) referenced to monomers is then given as:

$$\Delta G(n) = n \sum_{i=1}^{k} v_{i\alpha}\left(\mu^q_i - \mu^\beta_i\right) + \sigma A(n) \tag{6}$$

where μ^p_1 is the chemical potential of i single particles (atoms) in the ambient p phase.

The ordinary continuity equation which describes the time evolution of the distribution function (or number density) of clusters with size n in the cluster size space (this "space" is the set of integers, which describe the sizes of clusters in the system.) is given as:

$$\frac{\partial f(n,t)}{\partial t} = -\nabla J \tag{7}$$

If only monomers are mobile, $\frac{\partial f(n,t)}{\partial t} = J_{(n-1)+(1),(n)} - J_{(n)+(1),(n+1)}$.

Here we extend the CD theory in the framework of Slezov [32,33] to allow for mobile clusters, and we assume clusters have finite diffusivity up to a cluster size of n_{max}. With this assumption, the continuity equation is the total fluxes that reach clusters of size n minus the total fluxes that leave clusters of size n, it requires to count all the possible kinds of cluster pairs related to clusters of size n. There are various possible formalisms attempting to describe the continuity equation in the literature [15,40,41,46,47]. Here we use a continuity equation with the form:

$$\frac{\partial f(n,t)}{\partial t} = \sum_{m=1}^{\min(n-1,n_{max})} J_{(n-m)+(m),(n)} - \sum_{m=1}^{n_{max},n+m\le n_{total}} J_{(n)+(m),(n+m)} - \sum_{m=1}^{n_{total}-n} J_{(m)+(n),(m+n)} \tag{8}$$

where $J_{(n)+(m),(n+m)}$ is the flux from clusters of size n to clusters of size $n+m$, and n_{total} is the total number of cluster classes considered during the simulation. If all the clusters are diffusive, then the continuity

equation is given as:

$$\frac{\partial f(n,t)}{\partial t}=\sum_{m=1}^{n-1}J_{(n-m)+(m),(n)}-\sum_{m=1}^{n_{total}-n}J_{(n)+(m),(n+m)}-\sum_{m=1}^{n_{total}-n}J_{(m)+(n),(m+n)} \tag{9}$$

The first summation in Eqs. (8) and (9) takes into account all the possible reactions due to two clusters with sizes smaller than n that may generate clusters of size n. The second summation includes all the reactions of size n clusters with mobile clusters of size m to form $n+m$ sized clusters which may consume clusters of size n. The third summation accounts for the reactions of all the possible size of clusters that react with mobile clusters of size n and may induce a decrease in the number of clusters of size n. By combining these three terms together we can effectively account for all the clusters that are diffusive at the level of binary coalescence. But it should be noted that Eqs. (8) and (9) only consider the coagulation reactions of two particles to one and it is possible to add terms which include three or more particles coalescing to form another particle. However, for this work it is assumed that three or more particle coagulations are rare and can be neglected.

Note that Eqs. (8) and (9) naturally consider the fact that part of the particle size distribution for $n > n_{total}$ is not included in the numerical modeling. Thus, events that form particles with $n > n_{total}$ will not be treated correctly. Meanwhile, there are fluxes missing for n near n_{total} due to the boundary conditions used for computing. To reduce the impact of this limitation one should take $n_{total} \gg n_{max}$ to make sure the cluster size distribution function does not reach the region close to n_{total}. And one should also check that further increasing n_{total} has no influence on the simulated results.

In Eqs. (8) and (9), the flux term $J_{(n)+(m),\,(n+m)}$ has a corresponding definition to $J_{(n)+(1),\,(n+1)}$ given as:

$$J_{(n)+(m),(n+m)}=w^{(+)}_{(n)+(m),(n+m)}f(n,t)-w^{(-)}_{(n+m)-(m),(n)}f(n+m,t) \tag{10}$$

where the coefficient $w^{(+)}_{(n)+(m),(n+m)}$ is the rate of clusters of size n that absorb single mobile clusters of size m to form clusters of size $n+m$, and $w^{(-)}_{(n+m)-(m),(n)}$ is the rate of clusters of size $n+m$ emit single mobile clusters of size m to degrade to clusters of size n.

In Eq. (10), clusters with size m must be diffusive, otherwise the equations do not make sense. In the case where both the two reactants are mobile, the fluxes $J_{(n)+(m),\,(n+m)}$ and $J_{(m)+(n),\,(m+n)}$ are the fluxes of cluster reaction between mobile clusters of size n and m to clusters of size $n+m$ by processes involving each cluster as mobile. Specifically, $J_{(n)+(m),\,(n+m)}$ involves forming clusters of size $n+m$ by clusters of size n absorbing single mobile clusters of size m and forming clusters of size n by clusters of size $n+m$ emitting single mobile clusters of size m. Similarly, $J_{(m)+(n),\,(m+n)}$ involves absorbing and emitting single mobile clusters of size n. It should be noted that in this approach there appears to be double counting in cluster reactions as $(m)+(n)$, $(m+n)$ appears similarly to $(n)+(m)$, $(n+m)$, but they represent different flux terms as the order in the second index specifies which cluster is mobile. Thus, there is no double counting in the overall fluxes.

As in the case where only monomers are diffusive, the absorption coefficient is again defined as the rate of the considered mobile particles near the surface of precipitate reaching the precipitate interface by one step of motion. However, the absorption process is considered separately for each mobile species for simplification. In other words, each absorption coefficient only including the diffusivity of one class of clusters. Following the previous approaches [15,46], Eq. (2) is now extended for mobile clusters, and we define the absorption coefficient $w^{(+)}_{(n)+(m),(n+m)}$ as:

$$w^{(+)}_{(n)+(m),(n+m)}=4\pi R^2\frac{D^*_m}{\alpha_{m\beta}}c_{m\beta}\left\{\frac{1}{1+\left[\left(\frac{D^*_m}{D_{(m)}}\right)\left(\frac{R}{\alpha_{m\beta}}\right)\right]}\right\} \tag{11}$$

where R is the capture radius approximated as the sum of cluster radii $(R_n + R_m)$ [40,48], D^*_m is the diffusivity of clusters with size m near the precipitate/matrix interface, $\alpha_{m\beta}$ is the particle radius of clusters of size m in the matrix phase or more precisely the characteristic length scale, $c_{m\beta}$ is the volume concentration of clusters of size m defined analogous to $c_{1\beta}$, and $D_{(m)}$ is the diffusivity of mobile clusters of size m in the bulk. When R_m is negligible, the capture radius term can be approximated as R_n or one may want to use R_n initially. Following the detailed balance assumption as used in the case of monomers are diffusive, the emission coefficient $w^{(-)}_{(n+m)-(m),(n)}$ is given as:

$$w^{(-)}_{(n+m)-(m),(n)}=w^{(+)}_{(n)+(m),(n+m)}\exp\left(\frac{\Delta G_m(n+m)-\Delta G_m(n)}{k_BT}\right) \tag{12}$$

where $\Delta G_m(n)$ is the Gibbs free energy of formation of clusters with size n from clusters with size m, and is defined as:

$$\Delta G_m(n)=G(n)-\frac{n}{m}G(m) \tag{13}$$

where $G(n)$ is the free energy of clusters with size n.

If we insert Eq. (13) into Eq. (12), the following relation is obtained:

$$w^{(-)}_{(n+m)-(m),(n)}=w^{(+)}_{(n)+(m),(n+m)}\exp\left(\frac{G(n+m)-G(n)-G(m)}{k_B}T\right) \tag{14}$$

Furthermore, consider the similar definition of $G(n)$ that consistent with Eqs. (5) and (6), that is $G(n)=n\sum_{i=1}^{k}\nu_{i\alpha}\mu_i^a+\sigma A(n)$ for $n>1$. Then we have:

$$w^{(-)}_{(n+m)-(m),(n)}=w^{(+)}_{(n)+(m),(n+m)}\exp\left(\frac{\sigma A(n+m)-\sigma A(n)-\sigma A(m)}{k_B}T\right) \tag{15}$$

Like the derivation of Eq. (3), here we consider the diffusion-limited phase transition kinetics and according to Eq. (11),

$$w^{(+)}_{(n)+(m),(n+m)}\approx 4\pi(R_n+R_m)D_{(m)}c_{m\beta} \tag{16}$$

When we treat $f(n,t)$ as the number of clusters per unit site (atomic) volume of the matrix phase, then $c_{m\beta}$ becomes $f(m,t)/\Omega$. And the flux $J_{(n)+(m),\,(n+m)}$ is now:

$$J_{(n)+(m),(n+m)}=4\pi(R_n+R_m)\frac{D_{(m)}}{\Omega}f(m,t)f(n,t)-4\pi(R_n+R_m)\frac{D_{(m)}}{\Omega}\exp\left(\frac{G(n+m)-G(n)-G(m)}{k_B}T\right)f(m,t)f(n+m,t) \tag{17}$$

In this paper, we treat the free energy changes in cluster reactions with only monomers are mobile ($n_{max}=1$) as follows to introduce the solubilities of monomers to the equations:

$$\Delta G(n+1)-\Delta G(n)=\sum_{i=1}^{k}\nu_{i\alpha}\left(\mu_i^a-\mu_i^\beta\right)+\sigma A(n+1)-\sigma A(n) \tag{18}$$

Neglecting the Gibbs-Thomson effect on phase equilibrium, we have the phase equilibrium condition: $\mu_i^a=\overline{\mu}_i^\beta$, where $\overline{\mu}_i^\beta$ is the chemical potential of i atoms in the matrix phase at equilibrium. The activities of solutes in dilute matrix solution can be treated approximately following

the Henry's law. Then we can obtain the following relationship between emission and absorption coefficients:

$$w^{(-)}_{(n+1)-(1),(n)} = w^{(+)}_{(n)+(1),(n+1)} \frac{\prod_{i=1}^{k} \bar{x}_{i\beta}^{\nu_{i\alpha}}}{\prod_{i=1}^{k} x_{i\beta}^{\nu_{i\alpha}}} exp\left(\frac{\sigma A(n+1) - \sigma A(n)}{k_B T}\right) \quad (19)$$

where $\bar{x}_{i\beta}$ is the solubility limit of i in the matrix phase according to phase diagram. $\frac{\prod_{i=1}^{k} \bar{x}_{i\beta}^{\nu_{i\alpha}}}{\prod_{i=1}^{k} x_{i\beta}^{\nu_{i\alpha}}}$ in Eq. (19) represents the chemical contribution to the precipitation process. Similar treatments are also done for other cluster reactions including a monomer. Note in an alternative way, the chemical potential can be directly calculated from the CALPHAD type of thermodynamic database [49,50].

Of course, we may also assume monomers with α structure form in the matrix first before entering the precipitates, the formed monomers with α structure should be in (local) equilibrium with that in the matrix: $\sum_{i=1}^{k} \nu_{i\alpha}(\mu_i^{\alpha} - \mu_i^{\beta}) = -\sigma_1 A(1)$ with σ_1 is the composition dependent specific interfacial energy of α structured monomers. σ_1 then plays a role similar as the chemical driven force for phase transformation and should be distinguished from σ. Then, Eq. (15) can be uniformly used.

As done in some other previous works [40,46,47], in Eq. (11) one can use the sum diffusivity $(D_{(m)} + D_{(n)})$ instead of $D_{(m)}$, and similarly $(D_m^* + D_n^*)$ for D_m^*. In that case, Eq. (8) or (9) is suggested to be used as continuity equation with modification, that is a scale factor of 1/2 for $J_{(n)+(m),\,(n+m)}$ if both clusters n and m are mobile (both $D_{(m)} > 0$ and $D_{(n)} > 0$). In this way, Eqs. (8) and (9) can recover to the case when only monomers are diffusive. However, the model will be more sensitive to interfacial energy.

One should notice that the situation for clusters with mobility is similar to the case that the number of particles in a structure unit $n_b = m$ as described by Slezov [32] to generalize the CD theory to multicomponent precipitation. We can define different cluster size spaces denoted with structure units (n_bs). In n_b cluster size space, all cluster reactions will include a n_b sized mobile cluster (structure unit). The $n_b = 1$ cluster size space is that where only monomers are mobile. The behavior of cluster reactions in $n_b \neq 1$ cluster size spaces is analogous to that where only single particles (atoms or monomers) are mobile since the number of structure units n_u ($n_u = n/n_b$) only changes by 1 for each reaction. Thus, the properties of $n_b = 1$ cluster size space is also followed by other cluster size spaces. So, the generalization of the formalism and relationship between emission coefficients and absorption coefficients (Eqs. (11) and (12)) are reasonable.

The above complete a derivation of the extended version of the Slezov's CD theory to mobile clusters. The new CD model should be applicable for both diffusion-limited and kinetically-limited kinetics, as well as mobile clusters and multi-component (species) stoichiometric phase precipitation. In addition, this model is also useful for modeling pure coagulation process where there is no phase transition.

Finally, it is worth clarifying that one may want to follow the Binder's definition of flux [41] ($J_{(n)+(m),\,(n+m)} = u^{(+)}_{(n)+(m),(n+m)} f(n,t) f(m,t) - u^{(-)}_{(n+m)-(m),(n)} f(n+m,t)$), with the detailed balance assumption, if the reference state of formation energy is always taken as the state of the absorbed clusters as done in the present work and in the classical nucleation theory, then the same formula as Eq. (17) will be derived. The only difference is that the absorption coefficients need to be defined as: $u^{(+)}_{(n)+(m),(n+m)} = 4\pi(R_n + R_m)\frac{D_{(m)}}{\Omega}$, and the emission coefficients is then given as: $u^{(-)}_{(n+m)-(m),(n)} = 4\pi(R_n + R_m)\frac{D_{(m)}}{\Omega} \exp(\frac{G(n+m) - G(n) - G(m)}{k_B T})$ $f(m,t)$. Moreover, the presently extended CD theory in the case of diffusion-limited kinetics is different with that by Clouet et al. [40] and Jourdan et al. [15] by a factor term $f(m,t)$ in the emission part of the flux ($J_{(n)+(m),\,(n+m)}$).

3. Modeling Cu precipitation in Fe-Cu alloys

3.1. Simulation methods

The set of coupled ordinary differential equations which govern the temporal evolution of the distribution functions of Cu clusters in the CD theory, as described in Section 2, are solved by the CVODE solver in the SUNDIALS software package [51]. The emission coefficients for cluster reactions that can emit clusters containing >5 atoms (see Eq. (17)) are eliminated from the simulation work to speed up the calculations, since the emission rates of these larger clusters are negligible, and tests have shown that they have no impact on the simulation results.

3.2. Model parameters for Cu precipitation in Fe-Cu alloys

The major parameters for the model, as discussed in Section 2 with regards to Fe-Cu dilute alloys, are the diffusivity of Cu, diffusivity of Cu clusters, the solubility of Cu in Fe matrix, interfacial energy between the precipitates and the matrix phase, and the lattice parameter of Fe matrix. In this section, these parameters are discussed and/or determined from the literature information.

The diffusivity of Cu in dilute Fe-Cu alloys as an important input parameter that controls the mass transportation is analyzed first. In this work, diffusivity of Cu is taken the value of its impurity diffusivity as discussed before. All the original experimental measurements of impurity diffusivity are critically reviewed, and the experimental data are replotted in Fig. 1. The reported data from refs. [52–61] are consistent in the whole range of the measurement temperatures and are considered as reliable data. The earlier data from Lindner and Karnik [62] and Anand and Agarwala [63] did not show any apparent change of diffusion coefficient at Fe bcc_A2/fcc_A1 transition temperature, which is quite unreasonable to the knowledge of the present authors. While the data from Lazarev and Golikov [64] showed a less significant change at this transition temperature compared to the group we have identified as reliable data. Thus, these data in refs. [62–64] are neglected in the present evaluation. The experimental measurements are all at above 600 °C which is much higher than that often of interest for modeling CRPs evolution, e.g., the operation temperature of RPVs is about 300 °C, so some low temperature guidance on reliable values are useful, as discussed below.

In the previous modeling works, the diffusivity of Cu is either taken as a fitting parameter [7,10,12,16], taken the fitting value from a

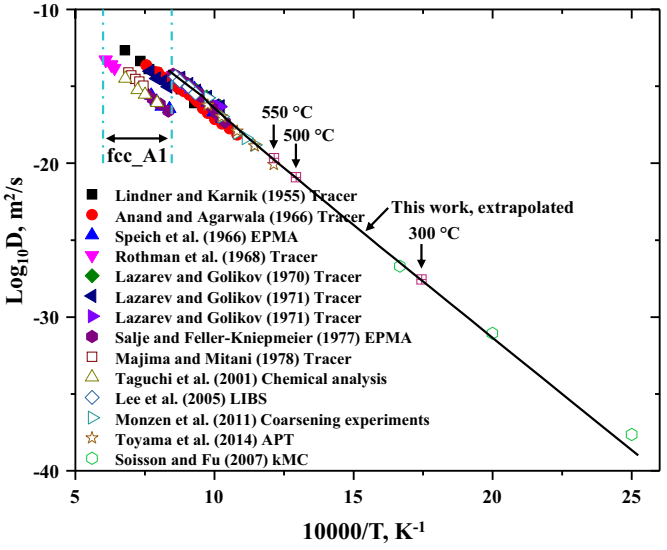

Fig. 1. Impurity diffusivity of Cu in Fe (EPMA: electron probe microanalysis; LIBS: laser induced breakdown spectrometry; APT: atom probe tomography).

previously modeling work [14,19,20], derived from the fitting of high temperature diffusivity data [11,17], taken as two times of Fe self-diffusivity [9,21], or taken as 3.56×10^{-22} m^2/s at 500 °C [15]. In the present work, the diffusivity is extrapolated from the reliable high temperature diffusivity data and takes into consideration of the atomistic kMC simulation data [25] at low temperature, since these data are also considered to be fairly reliable. The diffusivity of Cu in Fe used in the present work is also shown in Fig. 1 indicated by the extrapolated solid line, and can be approximated using an empirical equation suggested by Ruch et al. [65] as $D_{Cu} = 3.3 \times 10^{-3} \exp\left(\frac{-2.73}{k_B}T - \frac{\alpha M^2}{k_B}T\right)$ m^2/s, where α is about 0.1 to 0.2 eV and M is the magnetic long range order parameter available from Crangle and Goodman [66]. In this work, the α value of 0.15 eV is used to calculate Cu diffusivity, as the calculated value passes through the reliable data sets identified above and also is close to the low temperature kMC results [25].

Binder et al. [67,68] approximated the diffusivity of mobile clusters as $D_{(n)} = D_{(1)} n^{-\frac{4}{3}}$. The model was modified by Soisson and Fu [25] based on their atomistic kMC simulation data for cluster sizes up to 150 atoms. Unfortunately, the modified model substantially overestimates the atomistic kMC simulation data at small cluster size. Here, the diffusivity of Cu clusters is taken from the modified model by Soisson and Fu [25] for larger clusters, and the diffusivity for smaller particles is fitted to the atomistic kMC simulation results [25] using an exponential function. The diffusivity of clusters is then given as:

$$D_{(n)} = \min(D_1, D_2) \tag{20}$$

and D_1 and D_2 are presented as:

$$D_1 = D_{Cu} n^{\exp(-0.0049T + 3.28)}$$

$$D_2 = 7.14 \times 10^{-5} \exp\left(\frac{-2.65}{k_B}T\right) \exp\left(\frac{0.7}{k_B T}\right) n^{-\frac{4}{3}}$$

Fig. 2 shows the calculated cluster mobilities of Cu according to Eq. (20) compared with the atomistic kMC simulation results [25] at different temperatures. The predicted Cu cluster diffusivities by Eq. (20) are used in the current simulations with small adjustments to fit specific data sets, as will be discussed in detail later.

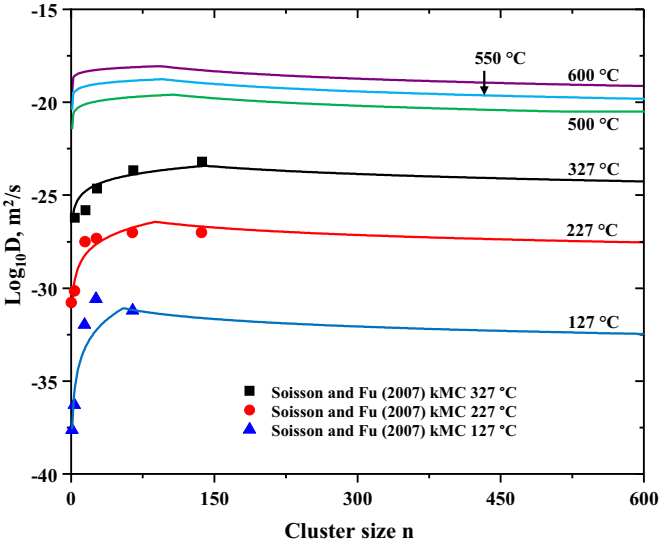

Fig. 2. Calculated Cu cluster mobilities by Eq. (20) along with the kMC simulation results [25].

The solubility of Cu varies during the precipitation process due to the bcc to 9R, 9R to 3R, and 3R to fcc phase transitions [69,70]. The solubility data of bcc Cu in bcc Fe solution is used and taken from the simulation work by Soisson and Fu [25], and given in mole fraction as $C_{Cu}^{sol}(Fe) = \exp(1)\exp\left(\frac{-0.545}{k_B}T\right)$. The model fit is most accurate for bcc Cu precipitates which occur up to about 4 nm in diameter. Bcc Cu precipitates are common in the important application of RPV steels and other precipitate strengthening Fe-Cu based steels, the most relevant for initial stage of precipitation, and represent the sizes seen during most of the time scales being modeled in the present work (provided one considers the time in logarithm units). The approximation that phase transitions of the precipitates have only modest quantitative effect on the growth in the domains studied is therefore made in the present work.

According to the literature, the interfacial energy for Cu precipitates in bcc_A2 solution is still poorly constrained. The interfacial energy used in the literature for various precipitation simulations in the Fe-Cu dilute alloys varies from 0.15 to 1.2 J/m^2 [9]. Theories that are generally used to predict the temperature dependence of interfacial energy for solid-solid interface including the Cahn-Hilliard theory [71] and the generalized near-neighbor broken-bond theory [72], however, these two theories can give quite different temperature dependent interfacial energy [9,71]. It is also reasonable to consider the cluster size dependence of the interfacial energy as described by Tolman [73]. Since the Cu interfacial energy is poorly constrained and of critical importance, here interfacial energy is treated as an adjustable parameter and the cluster size dependence is neglected for simplification.

The lattice constant of dilute bcc Fe-Cu alloys is taken as 0.287 nm [74,75].

3.3. Effects of model parameters on precipitation kinetics

In this section, the effects of interfacial energy, diffusivity, Cu solubility, initial Cu concentration in the matrix, and n_{max} on the precipitation properties (matrix concentration, mean cluster radius, precipitate number density, and precipitate volume fraction) are examined for the current CD model under isothermal condition. Since there are many experimental measurements of Cu precipitates in Fe-Cu alloys with Cu content close to 1.34 at.% at 500 °C in the literature [7,8,10,22,76–81], here Fe-1.34 at.% Cu alloy is used as a model alloy for the study. Unless specified, the simulation condition within this section will be the values presented in Table 1. When parameters are explored, they generally encompass the typical ranges seen in the literature. In many cases we compare parameter ranges for only mobile monomers ($n_{max} = 1$) and for mobile clusters ($n_{max} > 1$). Ranges of other parameters in such comparisons may vary as we attempted to keep the physical behavior similar and the model stable across such comparisons, both of which aspects can be altered significantly by changes in n_{max}. It is worth notifying that $n_{max} = 50$ maybe not a good approximation for Fe-Cu alloys since clusters containing >50 Cu atoms are still highly mobile (see Fig. 2). However, given the large number of runs needed to explore the parameters studied in this section it is necessary to reduce the computational time by a modest n_{max}. As the studies presented in this section are just testing the effects of model parameters in the cases of mobile monomers and mobile clusters, a highly accurate representation of Cu cluster kinetics is not necessary. In this section, only clusters

Table 1
Model parameters utilized to study the CD model.

Temperature (°C)	500
Alloy composition (at.%)	1.34
Interfacial energy of Cu precipitates (J/m^2)	0.50
Diffusivity of Cu monomers (m^2/s)	1.55×10^{-21}
bcc Cu solubility limit in bcc Fe (at.%)	0.076 [25]
Up limit of the size of mobile clusters, n_{max} (atoms)	50

containing >64 atoms are counted when determining number density, mean radius, and volume fraction, consistent with limitations of many experimental measurements and following the approach of ref. [18].

3.3.1. Interfacial energy

The critical nucleus size, nucleation rate, growth rate, and coarsening rate are interfacial energy dependent [82,83]. The effect of interfacial energy is studied by varying it from 0.1 to 0.8 J/m^2 for $n_{max} = 1$ and from 0.38 to 0.54 J/m^2 for $n_{max} = 50$. The simulated results are given in Figs. S2 and S3 in the Supplementary data. For both $n_{max} = 1$ and $n_{max} = 50$, increasing interfacial energy severely delays the depletion process of Cu content in the matrix phase and increases the growth rate. The mean radius also increases more steeply with annealing time as interfacial energy increases due to the increased growth rate. For $n_{max} = 1$ the peak number density increases as interfacial energy varies from 0.1 to 0.3 J/m^2 and the number density sprout time shifts to a limit value of about 2000 s. Further increase in interfacial energy induces a reduction in number density due to the large energy barrier to form precipitates. The volume fraction of precipitates shows the similar trend as number density with varying interfacial energy.

There are plateaus in the diagrams for intermediate interfacial energy (0.35 to 0.45 J/m^2) for $n_{max} = 1$. In particular, the first plateau in the Cu concentration profile occurs because a population of small clusters has reached a "near equilibrium" with the monomers in the matrix, the monomer concentration does not change that much. The precipitates then grow by coarsening. Eventually they reach a large enough size their surface energy contribution drops significantly, and the system is once again in supersaturation, and the Cu concentration starts to decrease again. For example, this occurs between times 10^2 and 10^4 s for interfacial energy 0.4 J/m^2. This process is hard to observe in the number density, mean radius, and volume fraction plots in Fig. S2(b) to (d) since these properties are only calculated for clusters with >64 atoms, which is larger than these initial small clusters that undergo coarsening. This early stage coarsening prediction is consistent with the experimental observations of coarsening at early stage by Hornbogen [84]. For the interfacial energy (0.35 to 0.45 J/m^2), the nucleation, growth, and coarsening dominated regions can be identified from the mean radius evolution profile, since there are clear regions where mean radius $\overline{R}$ scales with time as $\overline{R} \propto t^{\frac{1}{2}}$ (growth dominated) and $\overline{R} \propto t^{\frac{1}{3}}$ (coarsening dominated). In addition, the plateau in the radius and number density indicates that there is a separation between times with significant nucleation and coarsening, i.e., a time during which neither is very active [82]. For example, for interfacial energy 0.4 J/m^2, during about 10^5 to 10^6 s there is little significant nucleation or coarsening. Note that the onset of strong coarsening near 10^6 s is not inconsistent with the coarsening at earlier times of 10^2 to 10^4 s described above, as this later time coarsening occurs in a different regime for much larger particles. For low interfacial energy, i.e. ≤0.3 J/m^2, nucleation and coarsening regions overlap with each other. The current model shows similar features as the model developed based on classical nucleation theory [82].

The surface energy dependence of precipitation kinetics is substantially altered by the introduction of cluster mobility. Increasing interfacial energy with mobile clusters still has strong impact on the volume fraction and concentration profiles and leads to shape change in the profiles. The number density and mean radius are less severally affected.

3.3.2. Diffusivity

Both emission coefficients and absorption coefficients contain diffusivity in the CD theory. The flux term $J_{(n)+(m),\,(n+m)}$ is proportional to the diffusivity $D_{(m)}$, thus the diffusivity of clusters critically controls the kinetics of precipitation. We perform simulations with $n_{max} = 1$ ($\sigma = 0.4$ J/m^2) and $n_{max} = 50$ ($\sigma = 0.5$ J/m^2) with a range of diffusion coefficients to study the effects of diffusivity on precipitation kinetics. The calculated results are shown in Figs. S4 and S5 of the Supplementary data. It is not surprising to see that the precipitation process is enhanced by increasing the diffusivity of clusters simultaneously to 3, 6, 9, and 12 times for both $n_{max} = 1$ and $n_{max} = 50$. The profile starting time and number density peaking time both shift to shorter time with increased diffusivity. There is no shape change for the mean radius, number density, and volume fraction versus time profiles when increasing diffusion coefficients, but only a shift of the profile to an earlier time. This is consistent with the former simulated results by Robson [82] using the KWN model based on classical nucleation theory. However, adding cluster mobility alters the precipitation kinetics since the diffusion of mobile clusters also can accelerate the precipitation process, this will be further discussed later. We can easily draw the conclusion that the starting time of mean radius, number density, and volume fraction profiles are very sensitive to diffusivity.

3.3.3. Solubility

The solubility of Cu in Fe matrix is the parameter that relates to the chemical driving force for Cu precipitation kinetics. As shown in Eq. (19), the solubility of Cu takes part in the equilibrium solution product ($\prod_{i=1}^{k} \bar{x}_{i\beta}^{\nu_{i\alpha}}$) and will have impact on the emission coefficients and reduce the related flux term. The model-predicted results assuming the solubility of Cu varies from 1 to 2 times the value from Table 1 are shown in Figs. S6 and S7 in the Supplementary data with $n_{max} = 1$ ($\sigma = 0.4$ J/m^2) and $n_{max} = 50$ ($\sigma = 0.5$ J/m^2) respectively. The general trends are the same for both cases, increasing the solubility will extend the $\overline{R} \propto t^{\frac{1}{2}}$ growth period, decrease the peak number density, and delay the volume fraction increase and Cu content depletion in the matrix. However, the change in solubility limit seems does not much alter the precipitation starting time. In addition, it is easy to see that the solubility limit will affect the overlapping between nucleation and coarsening since the plateau on number density profile is delayed and shortened with increased solubility. In general, solubility has strong influence on the shape of all the precipitation evolution parameters calculated.

3.3.4. Matrix composition

The supersaturation of solutes provides the chemical driving force for nucleation and crystallization. Thus, supersaturation is required for precipitation study. Supersaturation can be defined by either the difference or the ratio of instantaneous and equilibrium alloy composition in the matrix. It can be changed by modifying either or both the solute solubility and matrix alloy composition. Section 3.3.3 can therefore be considered as a study of the effect of changing supersaturation through changing solubility. Here, the alloy composition is varied to see the changes in terms of the four key properties describing precipitation evolution (a study of the effects of changing supersaturation through alloy composition). Figs. S8 and S9 in the Supplementary data show the calculated results with $n_{max} = 1$ ($\sigma = 0.4$ J/m^2) and $n_{max} = 50$ ($\sigma = 0.5$ J/m^2) respectively. When only monomers are diffusive, there is no noticeable precipitation in the time scale considered here for alloy with up to 0.6 at.% Cu. This limit is reduced by adding cluster mobility (for $n_{max} = 50$) to about 0.4 at.% Cu. Matrix composition not only affects the nucleation and growth rates but also influences the overlapping of nucleation and coarsening regimes. For example, for $n_{max} = 1$ clear plateau in the number density-time evolution profile can be seen for alloy composition of 1.0 and 1.2 at.% Cu but not others. However, these plateaus do not show up for the cases including cluster mobility. Enlarging the alloy composition as expected increases the peak number density, volume fraction of precipitates, and the alloy response to annealing for both $n_{max} = 1$ and $n_{max} = 50$. The precipitation kinetics is also enhanced by cluster mobility.

3.3.5. Cluster mobility

In metallic systems, it is generally thought that monomers are the only particles that are mobile during the precipitation process. This is true for some alloy systems like Al-Sc and Al-Zr [85]. However, as noted in Section 1, there are both theoretical and numerical evidences

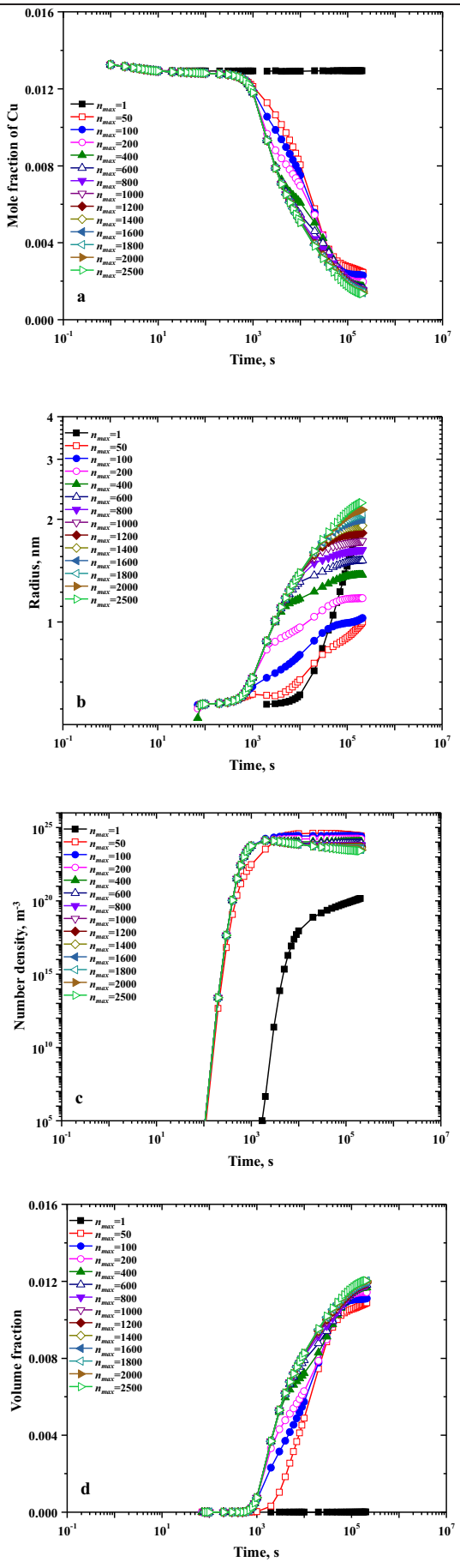

that monomers are not the only mobile particles in Fe-Cu alloys [9,15,25]. However, the exact size to which clusters are mobile is uncertain, as solute pinning, phase changes, and other factors might play increasingly important roles in cluster motion as size increases. Here we take n_{max} as a variable to check its influence on the kinetics of Cu precipitation in Fe-1.34 at.% Cu alloy at 500 °C.

Fig. 3 shows the calculated results with n_{max} from 1 to 2500. It can be notified from the diagram that the precipitation kinetics is substantially enhanced by cluster mobility. When only considering the mobility of monomers, the mean radius grows steeply and obeys the $\overline{R} \propto t^{\frac{1}{2}}$ law. However, the volume fraction and number density of precipitates are quite low compared to typical experimental results. With the introduction of cluster mobility, the matrix composition, mean radius, number density, and volume fraction evolution profiles are substantially modified. Precipitation initiates at a much earlier time. The mean radius and volume fraction also show shape change with enough variability. Importantly, the mean radius can follow the $\overline{R} \propto t^{\frac{1}{3}}$ growth law from early stage of precipitation, which is consistent with the experimental observations. Meanwhile, the number density of precipitates can be also modified with a much more reasonable peak value (about 10^{24} m^{-3}) and profile shape like that measured by experiments. The volume fraction of precipitates and Cu concentration in the matrix convergence to a limiting profile as n_{max} increases. A similar convergence happens at earlier times for mean radius and number density, but both continue to have n_{max} dependence for times later than a n_{max} dependent transition time $t_{tran}(n_{max})$.

The behavior of all the four precipitation properties can be understood by considering the impact of change in n_{max}. As n_{max} increases it adds more mobile cluster classes, which will generally increase the precipitation kinetics. However, the diffusivity of clusters given by Eq. (20) gradually increases with cluster size to a maximum value and then starts to decrease above about 100 to 150 atoms, for larger clusters the cluster diffusivity becomes so small that it is not significant on the time scales simulated here. This leads to the general asymptotic behavior with cluster size for any practical time. More importantly, larger clusters need time to form to contribute to the kinetics, which means that at earlier times larger mobile clusters play no role. This leads to essentially no dependence on increasing n_{max} for times short enough that the mobile cluster classes being added in the increase in n_{max} are not present. This effect sets the value of $t_{tran}(n_{max})$, which increases with n_{max} and leads to n_{max} increase independent behavior for progressively longer times as n_{max} increases. Note that due to the coupled impact of forming clusters and n_{max} on the precipitation properties, if the cluster diffusivity is changed the limiting profiles and $t_{tran}(n_{max})$ will also be different. This phenomenon is indeed diffusion-limited.

The effect of n_{max} on the time evolution of the cluster size distribution is also analyzed. The time evolution of the size distribution of clusters with $n_{max} = 50$ shows the similar general features as that with $n_{max} = 1$ (see Figs. S10 and S11 in the Supplementary data). However, there are discontinuity (kink) on the distribution profiles of the cases with $n_{max} = 50$ at about 0.52 nm which corresponds to a cluster size of 50 atoms. This is likely due to the sudden drop of cluster diffusion coefficient to zero at 50 atoms due to our use of $n_{max} = 50$. This kink is a boundary between mobile clusters and immobile clusters. It is therefore somewhat analogous to the role played by size 1 when $n_{max} = 1$. It is therefore not surprising that for longer times, the profiles started from this boundary show approximately the same feature as the whole profiles for the case $n_{max} = 1$.

Fig. 3. Effect of n_{max} on the time evolution of (a) matrix Cu concentration, (b) mean radius, (c) number density, and (d) volume fraction of Cu precipitates in Fe-1.34 at.% Cu alloy at 500 °C with interfacial energy of 0.5 J/m^2.

3.4. Results and discussions

3.4.1. Fe-near 1.34 at.% Cu and Fe-0.69 at.% Cu at 500 °C

Fe-Cu alloy with Cu content close to 1.34 at.% is widely used as a model alloy to study the precipitation kinetics in Cu containing steels at 500 °C [7,8,10,22,76–81,86]. As discussed before, it is impossible to model the precipitation properties simultaneously with only a physically reasonable Cu (monomer) diffusivity using either standard CD or KWN methods [8–10]. Here we try to use a physically meaningful Cu diffusivity to model the Cu precipitation behavior in Fe-1.34 at.% Cu alloy with the currently developed CD model by also considering the mobility of small clusters.

The available experimental information is summarized in Fig. 4. It can be seen from the diagram that the experimental number density and volume fraction are scatter but generally consistent except for the data from Warczok et al. [80] where very large number density was reported at very short aging time and the calculated volume fraction is also much larger compared to other works [8,10,76]. The measured mean radius from different authors is consistent at long annealing time (above 4×10^3 s). At short annealing time, the mean radii fall broadly into two groups. One group is represented by Kampmann and Wagner [8] and Perez et al. [22]. The other is Warczok et al. [80], Charleux et al. [79], and Osamura et al. [78]. Considering all the data, we believe that the experimental data from Warczok et al. [80] in the early stage of annealing has a large uncertainty. Indeed, it is very hard to control the annealing time to be as short as 200 s or less in a furnace and the samples may need some time to reach thermal equilibrium. Pre-existing precipitates may already form before the aging experiments, or very small clusters, which can be difficult to rigorously be identified as precipitates, were counted. Impurity presence could also be a reason for the fast kinetics in the early stage. Furthermore, maybe the small precipitates formed athermally at the initial stage or at very different condition which can also reach a very high number density.

Based on the results in Section 3.3, we select one set of parameters that can give a good description of all the precipitation properties in the time scale calculated up to 1.5×10^5 s. The parameters used are interfacial energy of 0.5 J/m^2, $n_{max} = 15000$, $D_{Cu} = 1.55 \times 10^{-21}$ m^2/s, and cluster diffusivity described by Eq. (20) with a cut off value of $10^{-20.5}$ $(2.04 \times D_{Cu})$ m^2/s for clusters containing >516 atoms. These parameters are also listed in Table 2. The use of the cut off value indicates that the cluster mobility as predicted by the modified model by Soisson and Fu [25] at large cluster size needs to be modified. In the CD theory, the calculations start from Cu as monomers, which is a useful consistent starting point but likely different from experiments, which are expected to start from some clustering. Following refs. [18, 87], clusters containing >44 atoms are considered to calculate the mean radius, number density, and volume fraction of Cu precipitates to be correct for the limited resolution of SANS and SAXS. It should be noted that, the value of this cut off has a dramatic effect on the mean radius and number density at short times when particles are very small (although, perhaps not on volume fraction since tests with a cut off of 10 atoms showed almost no impact on volume fraction values). The calculated results are also shown in Fig. 4, and even though the bcc to 9R phase change which happens at about the radius of 2 nm [69,70] is not considered, we can see the model-predicted results still match well with the reliable experimental data. This suggests that the developed model is suitable to model the precipitation behavior of Cu precipitates and the detailed phase transition can be neglected for the current purpose. However, it should be noted that we would need to further adjust model parameters (n_{max}, cluster diffusivity, etc.) to get good agreement between the simulated and experimental results at long time annealing (>1.5×10^5 s). At the very early stage, there is discrepancy between the calculated mean radius of 5 Å and the experimental one of 4 Å. The difference of 1 Å might depend on how rough or diffuse the interface is, or where you define as the edge of the particle, or how spherical it is in experiments, etc. The error of 1–2 Å in radius are likely not very meaningful.

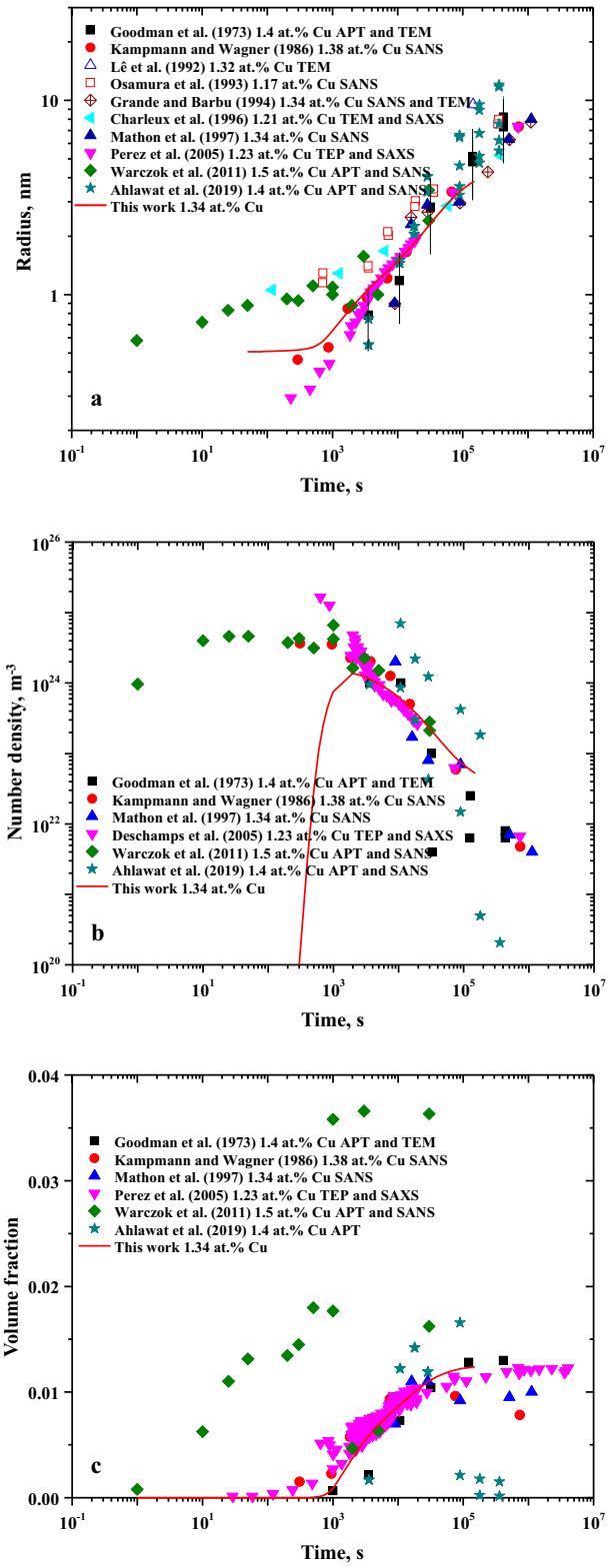

Fig. 4. Calculated time evolution of (a) mean radius, (b) number density, and (c) volume fraction of Cu precipitates in Fe-1.34 at.% Cu alloy at 500 °C compared with the experimental data (TEM: transmission electron microscopy; SANS: small angle neutron scattering; SAXS: small angle X-ray scattering; TEP: thermoelectric power).

The discrepancy in number density is very large, e.g. 10^3 s in Fig. 4 we have a number density of 10^{24} and the experimental value is 10^{25}, however this difference could be due in significant to the uncertainty in the measurement of number density. For example, the data from Ahlawat

Table 2
Model parameters utilized for the simulations.[a]

Temperature, °C	Interfacial energy, J/m^2	n_{max}, atoms	D_{Cu}, m^2/s $\alpha = 0.15$ eV	Cluster diffusivity, m^2/s
500	0.50	15,000	1.55×10^{-21}	From Eq. (20) for $n < 517$, else $2.04 \times D_{Cu}$
550	0.50	15,000	2.05×10^{-20}	From Eq. (20)
600	0.47	15,000	1.66×10^{-19}	From Eq. (20) for $n < 960$, else $0.24 \times D_{Cu}$

[a] Other parameters are from Section 3.2.

et al. [81] showed order of magnitude spread in number density for the same annealing time. Errors in number density may also occur when number density is determined indirectly from the measured mean radius and volume fraction, e.g. as occurred in the data from Perez et al. [22] and Deschamps et al. [86].

To demonstrate the obtained model parameters are useful in a relatively wide composition range, another simulation is carried out for Fe-0.69 at.% Cu alloy using the parameters for 500 °C from Table 2 and compared with the isothermal annealing data at the same temperature by Deschamps et al. [2,88]. The predicted results are shown in Fig. 5 with reasonable agreement in the simulated time range. This indicates that it is possible to model the precipitation kinetics of Cu precipitates for a range of composition at this temperature using a single set of parameters in the currently developed CD model.

3.4.2. Fe-0.977 and 1.14 at.% Cu at 550 °C

Two sets of experimental data are available at 550 °C with 0.977 and 1.14 at.% Cu respectively as shown in Fig. 6. There are apparent discrepancies in the two experiments in terms of mean radius, number density, and volume fraction. In the work of Buswell et al. [89], pre-existing large sized fcc precipitates were shown in the as-quenched microstructure before aging. The mean radius and number density of bcc Cu precipitates (small sized) measured by Buswell et al. [89] are consistent with that measured by He et al. [90] at long time annealing. The model predicted results are also shown in the figures for comparison. Since the data set itself shows certain unreasonable features like large number density and very small mean radius (<0.5 nm) at early stage precipitation which indicates possibly large experimental errors, no cut off value for cluster diffusivity is set. The measured volume fraction by He et al. [90] is quite suspicious since it did not reach the expected theoretical value at long time annealing which should be close to 0.0098 due to mass balance. Overall, the results already show quite reasonable agreement given the uncertainties and discrepancies in the data. The used model parameters are listed in Table 2.

3.4.3. Fe-1.23 at.% Cu at 600 °C

The precipitation kinetics of Cu precipitates in Fe-1.23 at.% Cu alloy at 600 °C was measured by Deschamps et al. [86] and Perez et al. [22] using TEP and SAXS. The simulated results are shown in Fig. 7 together with the experimental data. It can be seen from the diagram that the mean radius, number density, and volume fraction of precipitates are reasonably reproduced for time later than 10^3 s by the present model coupled with the optimized parameters in the simulated time scale. For times earlier than 10^3 s the model gets the correct volume fraction but too high in mean radius and too low in number density. The experimental number density was not measured directly but extracted from the measured mean radius and volume fraction. Therefore, the observed discrepancy just represents a discrepancy between the modeled and measured mean radius, although the source of this discrepancy is not clear. The used model parameters are listed in Table 2.

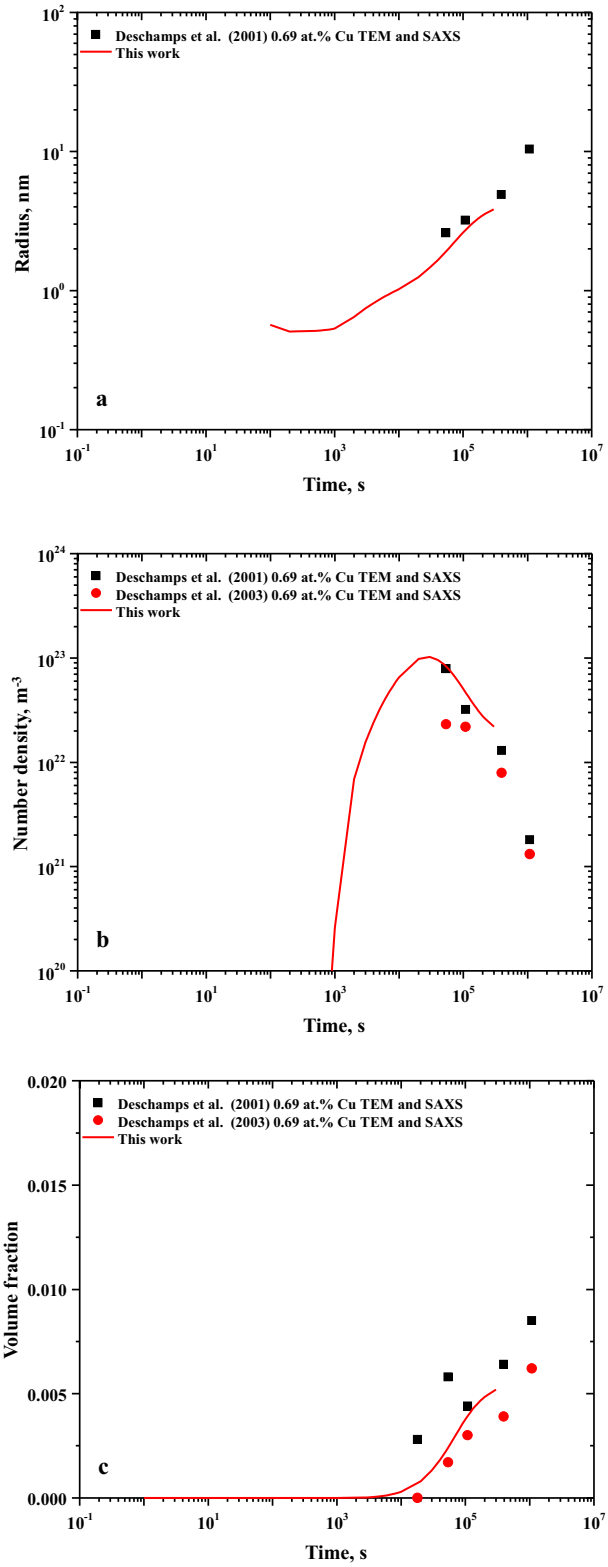

Fig. 5. Calculated time evolution of (a) mean radius, (b) number density, and (c) volume fraction of Cu precipitates in Fe-0.69 at.% Cu alloy at 500 °C compared with the experimental data.

4. Discussion on CRPs in Fe-Cu steels

The behavior of CRPs in multicomponent Fe-Cu steels is practically more important compared to pure Cu precipitates in binary Fe-Cu alloys. Alloying elements have strong interactions with CRPs in Fe-Cu based steels [3,88,89,91–101]. Both kinetics and thermodynamics can lead Mn, Ni, Al, and Si to segregate on the interface between CRPs and the matrix phase to form the core-shell or appendage type structures during the precipitation process [3,89,92–96,98,101]. The shells or

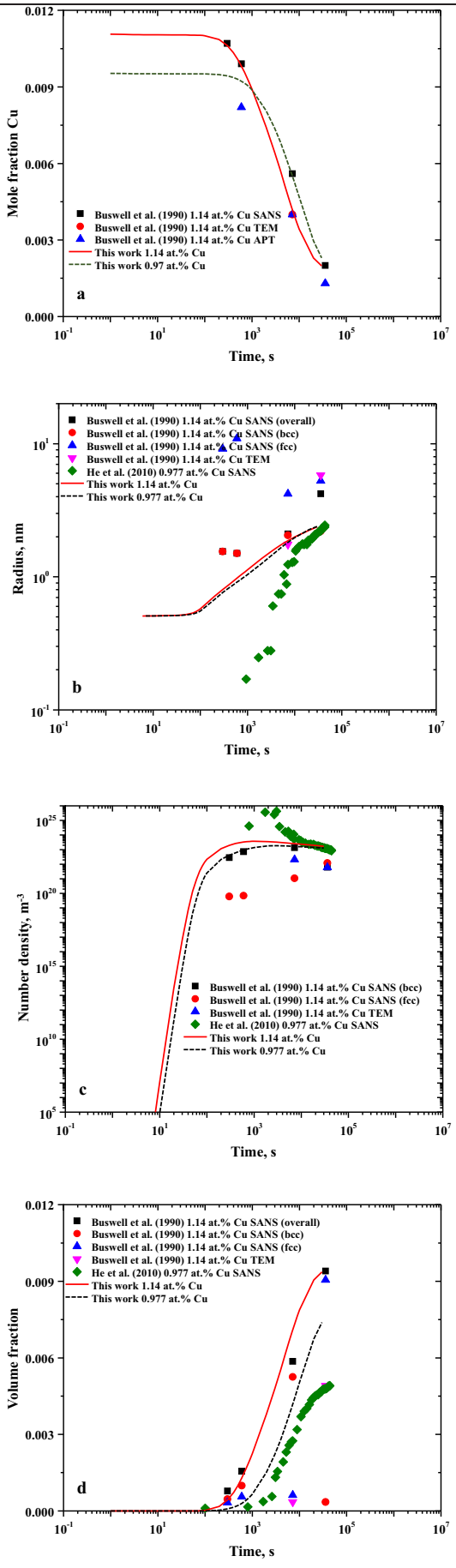

appendages, with chemical composition close to that of Mn-Ni containing binary or ternary phases, are important heterogeneous precipitates and we will be referred here as MNPs (Mn-Ni containing precipitates).

The precipitation kinetics of CRPs in multicomponent steels could be quite different due to the possible impurity pining and the shell or appendage structure formation. It is therefore interesting and of critical importance to quantitatively determine to what extent CRPs are still mobile when there is apparent segregation of solutes at precipitate/matrix interfaces. There is evidence that Mn, Ni, and C can accelerate the CRPs precipitation process [88,93,99,100] and the shells can decrease the interfacial energy of CRPs [3].

Unfortunately, the measurements of CRPs precipitation in Fe-Cu based steels under thermal annealing condition are still scarce. Here, we take 500 °C as an example to check the issue of possible loss of cluster mobility in multicomponent Fe-Cu based steels. A collection of the measured mean radius, number density, and volume fraction of precipitates in Fe-Cu based alloys are shown in Fig. 8. The precipitation kinetics showed strong composition dependence. The data from Osamura et al. [102] showed an accelerated precipitation due to the alloy element addition (the significantly larger radius than other studies suggests that maybe diameter was reported as radius), however, the number density of precipitates is still very similar to that in binary Fe-Cu alloys. There is difference in the measured mean radius by Isheim et al. [95,96,103] with about 1.2 at.% Cu. This difference could be due to the presence of Ni and Al. The addition of Al, Ni, Mn, and Si can apparently increase the total precipitates number density as can be seen by comparing the curves in Fig. 8 for Fe-Cu based alloys to pure Fe-Cu alloys (the line with n_{max} = 15,000). The measurements by Isheim et al. [3,95,96,103] exhibited slower coarsening kinetics compared to binary system and did not follow the $\overline{R} \propto t^{\frac{1}{3}}$ growth law as observed in Fe-Cu alloys. The recent atomistic simulation suggested that the delayed coarsening kinetics was because of the addition of Mn, Ni, and Si/P [30]. These changes in precipitation properties with alloying of pure Fe-Cu alloys indicate that either n_{max} is much smaller for CRPs precipitation in Fe-Cu based steels than Cu precipitation in Fe-Cu binary alloys at 500 °C, or the changes in kinetics are due to non-Cu containing precipitates formation.

Along with the experimental data on CRPs in Fig. 8, simulations for Fe-1.82 at.% Cu alloy (refers to the data from Kolli and Seidman [3]) with varying interfacial energy and n_{max} are carried out neglecting any role for other alloying elements. The predicted number density is broadly similar to the experimental data sets. However, the predicted mean radius can only reproduce the data by Kolli and Seidman [3] at short annealing time ($<10^5$ s) before Cu depletion in the matrix, and the predicted volume fraction is considerably smaller than the measured values. This result is consistent with the MNPs forming similarly to the precipitation of Cu in Fe-Cu binary alloys at early times but suggests significant deviation between pure Cu and CRP precipitate evolution at later times.

However, an examination of the experimental data from Buswell et al. [89] indicates that Ni addition (1.08 at.%) to Fe-1.13 at.% Cu alloy did not significantly alter the precipitation kinetics of CRPs. Meanwhile, the addition of Mn (1.05 at.%) in Fe-0.78 at.% Cu alloys can slow down the CRPs precipitation process at a low flux of irradiation [92]. In both cases, the mean radius evolution still follows the $\overline{R} \propto t^{\frac{1}{3}}$ law, which indicates the Cu cluster behavior qualitatively similar as in binary Fe-Cu alloys. These observations suggest that while there are most probably effective diffusivity and solubility changes, there is little evidence for large qualitative changes in the extent of mobile clusters in these ternary alloys.

Considering the experimental data [89,92,102], it is hard to make a judgement whether CRPs have different mobility compared to that in Fe-Cu dilute alloys. However, in general, the precipitation process in

Fig. 6. Calculated time evolution of (a) matrix Cu concentration, (b) mean radius, (c) number density, and (d) volume fraction of Cu precipitates in Fe-0.977 and 1.14 at.% Cu alloys at 550 °C compared with the experimental data.

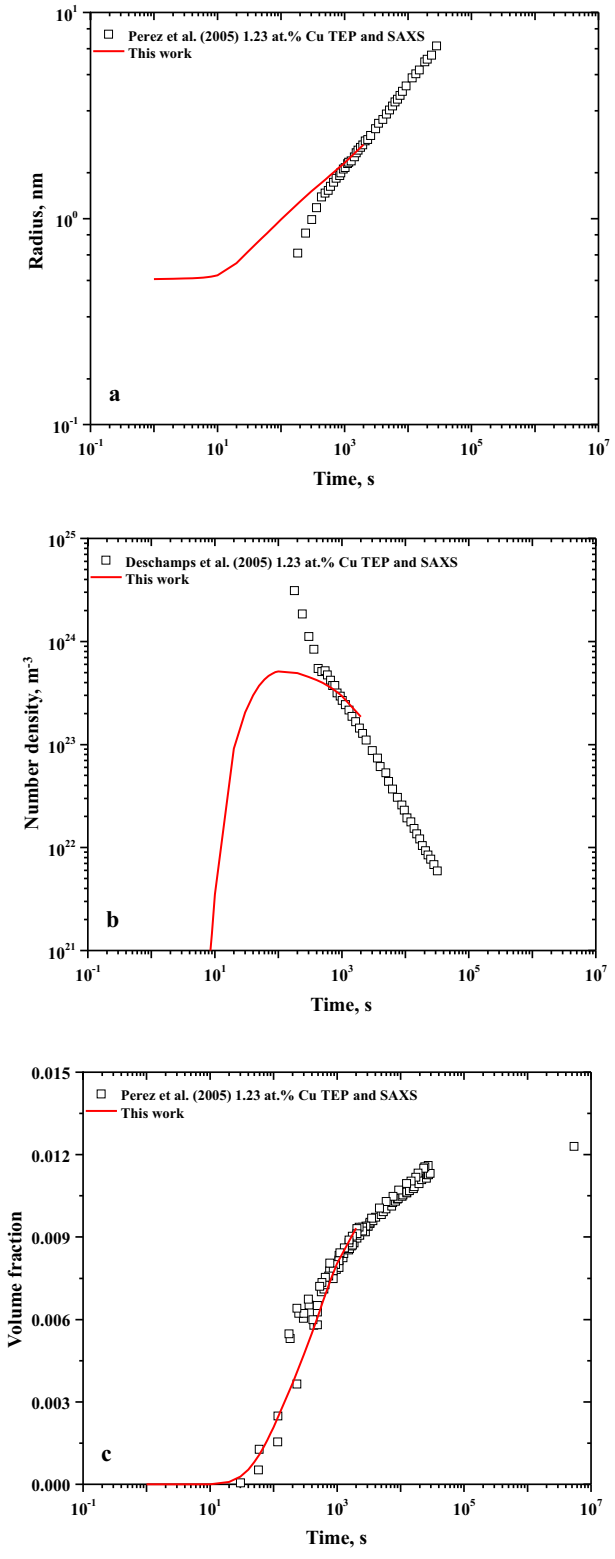

Fig. 7. Calculated time evolution of (a) mean radius, (b) number density, and (c) volume fraction of Cu precipitates in Fe-1.23 at.% Cu alloy at 600 °C compared with the experimental data.

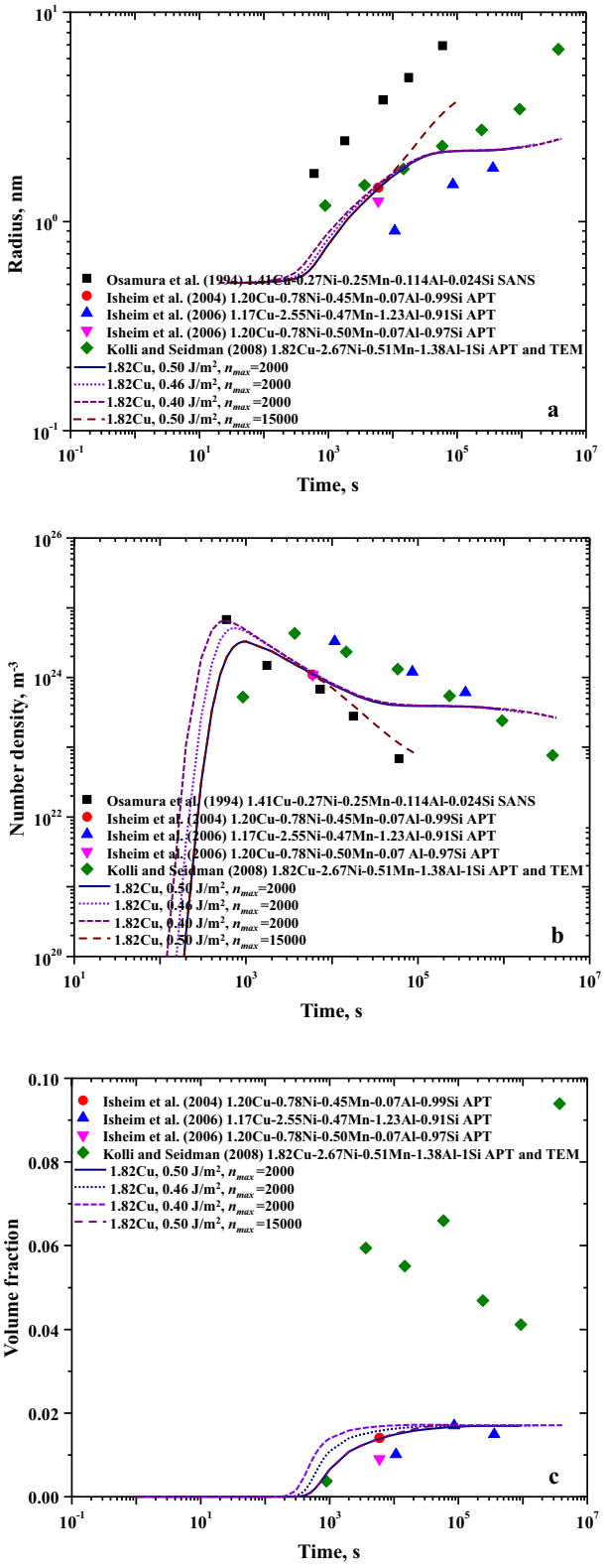

Fig. 8. Calculated time evolution of (a) mean radius, (b) number density, and (c) volume fraction of Cu precipitates in Fe-Cu based alloys at 500 °C compared with the experimental data.

multicomponent Fe-Cu based steels cannot be accurately modeled simply as binary Fe-Cu alloys but instead must be treated as a multicomponent multiphase precipitation problem. The interaction effects on solute solubility and the chemical stability of each precipitate phases in Fe-Cu based steels should be carefully studied for predictive precipitation model development for technical applications.

5. Summary and conclusions

This paper studied Cu precipitation in dilute Fe-Cu alloys under thermal annealing using the CD theory. The CD theory developed by Slezov

et al. was extended with cluster mobility. The effects of interfacial energy, diffusivity, solubility, matrix composition, and cluster mobility on the precipitation process of Cu precipitates were studied at 500 °C for the new model, and the causes of different trends were identified. When only monomers are diffusive, there is separation of nucleation, growth, and coarsening at high interfacial energy (≥0.3 J/m^2), and these three stages overlap at lower interfacial energy. With cluster mobility, no apparent separation of the three stages is observed in the simulated time scale. When all cluster (and monomer) diffusivities are simultaneously scaled by the same factor, it does not alter the shape of the simulated temporal evolution profiles, but instead only produces a shift along the time axis. Solubility and matrix composition will also affect the overlapping of nucleation and coarsening when only monomers are mobile. The general kinetic features of the current CD model are similar to that of the KWN model. Increasing n_{max} will eventually lead to a convergence of the time evolution profiles of precipitate volume fraction and Cu concentration in the matrix over all the time scales, and for a time below a n_{max} dependent cut off for mean radius and number density. The newly developed CD model with monomer and cluster mobility can simultaneously model the time evolution of the mean radius, number density, and volume fraction of Cu precipitates in dilute binary Fe-Cu alloys using physically reasonable input parameters. The optimized model parameters showed good prediction in a wide composition and temperature range, which indicates the developed model is suitable for dilute Fe-Cu alloys. Furthermore, we believe this model can serve as a foundation for modeling CRPs precipitation in RPVs under irradiation and other Fe-Cu based steels, although more assessments of the coupling of alloying elements with Cu precipitation kinetics would be needed. Analysis of the data for CRPs in Fe-Cu based steels indicated that alloying has a significant impact on the precipitation kinetics. This is likely due to at least changes in diffusivity and solubility, and it was not clear whether there were any changes in number of mobile cluster classes associated with alloying based on the limited available experimental information and our calculations.

CRediT authorship contribution statement

Senlin Cui: Conceptualization, Investigation, Writing - original draft, Writing - review & editing. **Mahmood Mamivand:** Formal analysis, Writing - original draft, Writing - review & editing. **Dane Morgan:** Conceptualization, Writing - original draft, Writing - review & editing, Supervision.

Declaration of competing interest

The authors declare that they have no known competing financial interests or personal relationships that could have appeared to influence the work reported in this paper.

Acknowledgements

This work has been supported by the U.S. Department of Energy Office of Nuclear Energy's Light Water Reactor Sustainability Program, Materials Aging and Degradation Pathway. We would like to also thank Prof. G. Robert Odette from University of California-Santa Barbara for extension helpful discussions related to the manuscript.

Appendix A. Supplementary data

Supplementary data to this article can be found online at https://doi.org/10.1016/j.matdes.2020.108574.

References

[1] T. Tsuchiyama, S. Yamamoto, S. Hata, M. Murayama, S. Morooka, D. Akama, S. Takaki, Plastic deformation and dissolution of ε-Cu particles by cold rolling in an over-aged particle dispersion strengthening Fe-2mass%Cu alloy, Acta Mater. 113 (2016) 48–55.
[2] A. Deschamps, M. Militzer, W.J. Poole, Precipitation kinetics and strengthening of a Fe-0.8 wt% Cu alloy, ISIJ Int. 41 (2001) 196–205.
[3] R.P. Kolli, D.N. Seidman, The temporal evolution of the decomposition of a concentrated multicomponent Fe-Cu-based steel, Acta Mater. 56 (2008) 2073–2088.
[4] S. Pizzini, K.J. Roberts, W.J. Phythian, C.A. English, G.N. Greaves, A fluorescence EXAFS study of the structure of copper-rich precipitates in Fe-Cu and Fe-Cu-Ni alloys, Philos. Mag. Lett. 61 (1990) 223–229.
[5] G.R. Odette, G.E. Lucas, Recent progress in understanding reactor pressure vessel steel embrittlement, Radiat. Eff. Defect S. 144 (1998) 189–231.
[6] G.R. Odette, R.K. Nanstad, Predictive reactor pressure vessel steel irradiation embrittlement models: issues and opportunities, JOM 61 (2009) 17–23.
[7] N.S.-D. Grande, A. Barbu, Study of Cu precipitation mechanisms in Fe-Cu 1.34 at.% alloy under electron irradiation, Radiat. Eff. Defect S. 132 (1994) 157–167.
[8] R. Kampmann, R. Wagner, Phase transformations in Fe-Cu alloys: SANS-experiments and theory, Springer Proc. Phys. 10 (1986) 73–77.
[9] G. Stechauner, E. Kozeschnik, Thermo-kinetic modeling of Cu precipitation in α-Fe, Acta Mater. 100 (2015) 135–146.
[10] M.H. Mathon, A. Barbu, F. Dunstetter, F. Maury, N. Lorenzelli, C.H. de Novion, Experimental study and modelling of copper precipitation under electron irradiation in dilute FeCu binary alloys, J. Nucl. Mater. 245 (1997) 224–237.
[11] A.V. Barashev, S.I. Golubov, D.J. Bacon, P.E.J. Flewitt, T.A. Lewis, Copper precipitation in Fe-Cu alloys under electron and neutron irradiation, Acta Mater. 52 (2004) 877–886.
[12] F. Christien, A. Barbu, Modelling of copper precipitation in iron during thermal aging and irradiation, J. Nucl. Mater. 324 (2004) 90–96.
[13] D. Xu, A. Certain, H.-J. Lee Voigt, T. Allen, B.D. Wirth, Ballistic effects on the copper precipitation and re-dissolution kinetics in an ion irradiated and thermally annealed Fe-Cu alloy, J. Chem. Phys. 145 (2016), 104704.
[14] X.-M. Bai, H. Ke, Y. Zhang, B.W. Spencer, Modeling copper precipitation hardening and embrittlement in a dilute Fe-0.3 at.% Cu alloy under neutron irradiation, J. Nucl. Mater. 495 (2017) 442–454.
[15] T. Jourdan, F. Soisson, E. Clouet, A. Barbu, Influence of cluster mobility on Cu precipitation in α-Fe: a cluster dynamics modeling, Acta Mater. 58 (2010) 3400–3405.
[16] S.I. Golubov, Y.N. Osetsky, A. Serra, A.V. Barashev, The evolution of copper precipitates in binary Fe-Cu alloys during ageing and irradiation, J. Nucl. Mater. 226 (1995) 252–255.
[17] S.I. Golubov, A. Serra, Y.N. Osetsky, A.V. Barashev, On the validity of the cluster model to describe the evolution of Cu precipitates in Fe-Cu alloys, J. Nucl. Mater. 277 (2000) 113–115.
[18] M. Mamivand, P. Wells, H. Ke, S. Shu, G.R. Odette, D. Morgan, CuMnNiSi precipitate evolution in irradiated reactor pressure vessel steels: Integrated Cluster Dynamics and experiments, Acta Mater. 180 (2019) 199–217.
[19] Q.L. Wang, J.Z. Zhao, A model describing the microstructure evolution in Fe-Cu alloys during thermal aging, Mater. Sci. Eng. A 528 (2010) 268–272.
[20] J.Z. Zhao, Q.L. Wang, H.L. Li, J. He, Modeling of the precipitation kinetics during aging a predeformed Fe-Cu alloy, Metall. Mater. Trans. A 42 (2011) 3200–3207.
[21] C. Zhang, M. Enomoto, T. Yamashita, N. Sano, Cu precipitation in a prestrained Fe-1.5 wt pct Cu alloy during isothermal aging, Metall. Mater. Trans. A 35 (2004) 1263–1272.
[22] M. Perez, F. Perrard, V. Massardier, X. Kleber, A. Deschamps, H. de Monestrol, P. Pareige, G. Covarel, Low-temperature solubility of copper in iron: experimental study using thermoelectric power, small angle X-ray scattering and tomographic atom probe, Philos. Mag. 85 (2005) 2197–2210.
[23] I.M. Lifshitz, V.V. Slyozov, The kinetics of precipitation from supersaturated solid solutions, J. Phys. Chem. Solids 19 (1961) 35–50.
[24] C. Wagner, Theory of precipitate change by redissolution, Z. Elektrochem. Angew. Phys. Chem. 65 (1961) 581–591.
[25] F. Soisson, C.-C. Fu, Cu-precipitation kinetics in α-Fe from atomistic simulations: vacancy-trapping effects and Cu-cluster mobility, Phys. Rev. B 76 (2007), 214102.
[26] F. Soisson, A. Barbu, G. Martin, Monte Carlo simulations of copper precipitation in dilute iron-copper alloys during thermal ageing and under electron irradiation, Acta Mater. 44 (1996) 3789–3800.
[27] N. Castin, M.I. Pascuet, L. Malerba, Modeling the first stages of Cu precipitation in α-Fe using a hybrid atomistic kinetic Monte Carlo approach, J. Chem. Phys. 135 (2011), 064502.
[28] Y. Wang, J. Yin, X. Liu, R. Wang, H. Hou, J. Wang, Precipitation kinetics in binary Fe-Cu and ternary Fe-Cu-Ni alloys via kMC method, Prog. Nat. Sci.-Mater. 27 (2017) 460–466.
[29] E. Vincent, C.S. Becquart, C. Pareige, P. Pareige, C. Domain, Precipitation of the FeCu system: a critical review of atomic kinetic Monte Carlo simulations, J. Nucl. Mater. 373 (2008) 387–401.
[30] G. Bonny, C. Domain, N. Castin, P. Olsson, L. Malerba, The impact of alloying elements on the precipitation stability and kinetics in iron based alloys: an atomistic study, Comput. Mater. Sci. 161 (2019) 309–320.
[31] L. Messina, N. Castin, C. Domain, P. Olsson, Introducing ab initio based neural networks for transition-rate prediction in kinetic Monte Carlo simulations, Phys. Rev. B 95 (2017), 064112.
[32] V.V. Slezov, Kinetics of First-order Phase Transitions, Wiley-VCH, Berlin, 2009.
[33] V.V. Slezov, J. Schmelzer, Kinetics of formation and growth of a new phase with a definite stoichiometric composition, J. Phys. Chem. Solids 55 (1994) 243–251.
[34] C. Liu, L. He, Y. Zhai, B. Tyburska-Püschel, P.M. Voyles, K. Sridharan, D. Morgan, I. Szlufarska, Evolution of small defect clusters in ion-irradiated 3C-SiC: combined cluster dynamics modeling and experimental study, Acta Mater. 125 (2017) 377–389.

[35] M. Volmer, Particle formation and particle action as a special case of heterogeneous catalysis, Z. Elektrochem. Angew. Phys. Chem. 35 (1929) 555–561.
[36] R. Becker, W. Döring, The kinetic treatment of nuclear formation in supersaturated vapors, Ann. Phys. (Berlin, Ger.) 24 (1935) 719–752.
[37] L. Farkas, The velocity of nucleus formation in supersaturated vapors, Z. Physik. Chem. 125 (1927) 236–242.
[38] J. Feder, K.C. Russell, J. Lothe, G.M. Pound, Homogeneous nucleation and growth of droplets in vapours, Adv. Phys. 15 (1966) 111–178.
[39] K.C. Russell, Nucleation in solids: the induction and steady state effects, Adv. Colloid Interf. Sci. 13 (1980) 205–318.
[40] E. Clouet, Modeling of nucleation processes, in: D.U. Furrer, S.L. Semiatin (Eds.), Fundamentals of Modeling for Metals Processing, ASM International 2009, pp. 203–219.
[41] K. Binder, Theory for the dynamics of "clusters." II. Critical diffusion in binary systems and the kinetics of phase separation, Phys. Rev. B 15 (1977) 4425–4447.
[42] S.L. Cui, L.J. Zhang, W.B. Zhang, Y. Du, H.H. Xu, Computational study of diffusivities in diamond Ge-Si alloys, J. Min. Metall., Sect. B 48 (2012) 227–249.
[43] S. Cui, L. Zhang, Y. Du, D. Zhao, H. Xu, W. Zhang, S. Liu, Assessment of atomic mobilities in fcc Cu-Ni-Zn alloys, CALPHAD 35 (2011) 231–241.
[44] G. Wilemski, The Kelvin equation and self-consistent nucleation theory, J. Chem. Phys. 103 (1995) 1119–1126.
[45] J. Frenkel, A general theory of heterophase fluctuations and pretransition phenomena, J. Chem. Phys. 7 (1939) 538–547.
[46] M.v. Smoluchowski, Versuch einer mathematischen theorie der koagulationskinetik kolloider lösungen, Z. Physik. Chem. 92U (1918) 129–168.
[47] P. Warczok, J. Zenisek, E. Kozeschnik, Atomistic and continuums modeling of cluster migration and coagulation in precipitation reactions, Comput. Mater. Sci. 60 (2012) 59–65.
[48] J. Lepinoux, Contribution of matrix frustration to the free energy of cluster distributions in binary alloys, Philos. Mag. 86 (2006) 5053–5082.
[49] S. Cui, I.-H. Jung, Thermodynamic modeling of the Cu-Fe-Cr and Cu-Fe-Mn systems, CALPHAD 56 (2017) 241–259.
[50] S. Cui, I.-H. Jung, Critical reassessment of the Fe-Si system, CALPHAD 56 (2017) 108–125.
[51] https://computing.llnl.gov/projects/sundials/publications.
[52] G.R. Speich, J.A. Gula, R.M. Fisher, in: M. Electron, T.D. McKinley, K.J. Heinrich, D.B. Witty (Eds.), Diffusivity and Solubility Limit of Copper in α- and γ-Iron, John Wiley and Sons, New York 1966, pp. 525–542.
[53] S.J. Rothman, N.L. Peterson, C.M. Walter, L.J. Nowicki, The diffusion of copper in iron, J. Appl. Phys. 39 (1968) 5041–5044.
[54] V.A. Lazarev, V.M. Golikov, Diffusion of copper in iron and its alloys, Fiz. Metal Metalloved. 29 (1970) 598–602.
[55] V.A. Lazarev, V.M. Golikov, Bulk and grain boundary diffusion of copper in iron and copper-iron alloys studied by using copper-64, Metod Izotop. Indikatorov Nauch. Issled. Prom. Proizvod. (1971) 65–69.
[56] G. Salje, M. Feller-Kniepmeier, The diffusion and solubility of copper in iron, J. Appl. Phys. 48 (1977) 1833–1839.
[57] K. Majima, H. Mitani, Lattice and grain boundary diffusion of copper in γ-iron, Trans. JIM 19 (1978) 663–668.
[58] O. Taguchi, M. Hagiwara, Y. Yamazaki, Y. Iijima, Impurity diffusion of Al and Cu in γ-Fe, Diffus. Defect Data, Pt. A 194-199 (2001) 91–96.
[59] C.-G. Lee, J.-H. Lee, B.-S. Lee, Y.-I. Lee, T. Shimozaki, T. Okino, Measurement of the impurity diffusivity of Cu in Fe by laser induced breakdown spectrometry, Diffus. Defect Data, Pt. A 237-240 (2005) 266–270.
[60] R. Monzen, K. Takada, K. Matsuda, Coarsening kinetics of Cu particles in an Fe-1.5% Cu alloy, Z. Metallkd. 94 (2003) 1241–1246.
[61] T. Toyama, F. Takahama, A. Kuramoto, H. Takamizawa, Y. Nozawa, N. Ebisawa, M. Shimodaira, Y. Shimizu, K. Inoue, Y. Nagai, The diffusivity and solubility of copper in ferromagnetic iron at lower temperatures studied by atom probe tomography, Scr. Mater. 83 (2014) 5–8.
[62] R. Lindner, F. Karnik, Diffusion von radioaktiven kupfer in technischem stahl, Acta Metall. 3 (1955) 297.
[63] M.S. Anand, R.P. Agarwala, Diffusion of copper in iron, J. Appl. Phys. 37 (1966) 4248–4251.
[64] V.A. Lazarev, V.M. Golikov, Diffusion of copper in iron and iron-boron and iron-molybdenum alloys, Fiz. Metal. Metalloved. 31 (1971) 885–886.
[65] L. Ruch, D.R. Sain, H.L. Yeh, L.A. Girifalco, Analysis of diffusion in ferromagnets, J. Phys. Chem. Solids 37 (1976) 649–653.
[66] J. Crangle, G.M. Goodman, Magnetization of pure iron and nickel, Proc. Roy. Soc., Ser. A 321 (1971) 477–491.
[67] K. Binder, D. Stauffer, Theory for the slowing down of the relaxation and spinodal decomposition of binary mixtures, Phys. Rev. Lett. 33 (1974) 1006–1009.
[68] K. Binder, D. Stauffer, Statistical theory of nucleation, condensation and coagulation, Adv. Phys. 25 (1976) 343–396.
[69] P.J. Othen, M.L. Jenkins, G.D.W. Smith, W.J. Phythian, Transmission electron microscope investigations of the structure of copper precipitates in thermally-aged Fe-Cu and Fe-Cu-Ni, Philos. Mag. Lett. 64 (1991) 383–391.
[70] P.J. Othen, M.L. Jenkins, G.D.W. Smith, High-resolution electron microscopy studies of the structure of Cu precipitates in α-Fe, Philos. Mag. A 70 (1994) 1–24.
[71] J.W. Cahn, J.E. Hilliard, Free energy of a nonuniform system. I. Interfacial free energy, J. Chem. Phys. 28 (1958) 258–267.
[72] B. Sonderegger, E. Kozeschnik, Generalized nearest-neighbor broken-bond analysis of randomly oriented coherent interfaces in multicomponent fcc and bcc structures, Metall. Mater. Trans. A 40 (2009) 499–510.
[73] R.C. Tolman, The effect of droplet size on surface tension, J. Chem. Phys. 17 (1949) 333–337.
[74] S.G.E. te Velthuis, J.H. Root, J. Sietsma, M.T. Rekveldt, S. van der Zwaag, The ferrite and austenite lattice parameters of Fe-Co and Fe-Cu binary alloys as a function of temperature, Acta Mater. 46 (1998) 5223–5228.
[75] L. Zwell, D.E. Carnahan, G.R. Speich, Lattice parameter of ferritic and martensitic Fe-Ni alloys, Metall. Trans. 1 (1970) 1007–1009.
[76] S.R. Goodman, S.S. Brenner, J.R. Low, An FIM-atom probe study of the precipitation of copper from iron-1.4 at. pct copper. Part I: field-ion microscopy, Metall. Trans. 4 (1973) 2363–2369.
[77] T.N. Lê, A. Barbu, D. Liu, F. Maury, Precipitation kinetics of dilute FeCu and FeCuMn alloys subjected to electron irradiation, Scr. Metall. Mater. 26 (1992) 771–776.
[78] K. Osamura, H. Okuda, M. Takashima, K. Asano, M. Furusaka, Small-angle neutron scattering study of phase decomposition in Fe-Cu binary alloy, Mater. Trans. JIM 34 (1993) 305–311.
[79] M. Charleux, F. Livet, F. Bley, F. Louchet, Y. Bréchet, Thermal ageing of an Fe-Cu alloy: microstructural evolution and precipitation hardening, Philos. Mag. A 73 (1996) 883–897.
[80] P. Warczok, D. Reith, M. Schober, H. Leitner, R. Podloucky, E. Kozeschnik, Investigation of Cu precipitation in bcc-Fe-comparison of numerical analysis with experiment, Int. J. Mater. Res. 102 (2011) 709–716.
[81] S. Ahlawat, S.K. Sarkar, D. Sen, A. Biswas, Revisiting temporal evolution of Cu-rich precipitates in Fe-Cu alloy: correlative small angle neutron scattering and atom-probe tomography studies, Microsc. Microanal. (2019) 1–9.
[82] J.D. Robson, Modelling the overlap of nucleation, growth and coarsening during precipitation, Acta Mater. 52 (2004) 4669–4676.
[83] R. Kampmann, R. Wagner, Kinetics of precipitation in metastable binary alloys - theory and application to copper-1.9 at.% titanium and nickel-14 at.% aluminum, Decompos. Alloys, Proc. Acta-Scr. Metall. Conf. 2nd ed. 1984, pp. 91–103.
[84] E. Hornbogen, The role of strain energy during precipitation of copper and gold from alpha iron, Acta Metall. 10 (1962) 525–533.
[85] E. Clouet, M. Nastar, C. Sigli, Nucleation of Al_3Zr and Al_3Sc in aluminum alloys: from kinetic Monte Carlo simulations to classical theory, Phys. Rev. B 69 (2004), 064109.
[86] A. Deschamps, C. Genevois, M. Nicolas, F. Perrard, F. Bley, Study of precipitation kinetics: towards non-isothermal and coupled phenomena, Philos. Mag. 85 (2005) 3091–3112.
[87] H. Ke, P. Wells, P.D. Edmondson, N. Almirall, L. Barnard, G.R. Odette, D. Morgan, Thermodynamic and kinetic modeling of Mn-Ni-Si precipitates in low-Cu reactor pressure vessel steels, Acta Mater. 138 (2017) 10–26.
[88] A. Deschamps, M. Militzer, W.J. Poole, Comparison of precipitation kinetics and strengthening in an Fe-0.8%Cu alloy and a 0.8%Cu-containing low-carbon steel, ISIJ Int. 43 (2003) 1826–1832.
[89] J.T. Buswell, C.A. English, M.G. Hetherington, W.J. Phythian, G.D.W. Smith, G.M. Worrall, An analysis of small clusters formed in thermally aged and irradiated iron-copper and iron-copper-nickel model alloys, ASTM Spec. Tech. Publ. 1046 (1990) 127–153.
[90] S.M. He, N.H. van Dijk, M. Paladugu, H. Schut, J. Kohlbrecher, F.D. Tichelaar, S. van der Zwaag, In situ determination of aging precipitation in deformed Fe-Cu and Fe-Cu-B-N alloys by time-resolved small-angle neutron scattering, Phys. Rev. B 82 (2010), 174111.
[91] S. Shu, P.B. Wells, N. Almirall, G.R. Odette, D.D. Morgan, Thermodynamics and kinetics of core-shell versus appendage co-precipitation morphologies: an example in the Fe-Cu-Mn-Ni-Si system, Acta Mater. 157 (2018) 298–306.
[92] S. Shu, B.D. Wirth, P.B. Wells, D.D. Morgan, G.R. Odette, Multi-technique characterization of the precipitates in thermally aged and neutron irradiated Fe-Cu and Fe-Cu-Mn model alloys: atom probe tomography reconstruction implications, Acta Mater. 146 (2018) 237–252.
[93] O.I. Gorbatov, Y.N. Gornostyrev, P.A. Korzhavyi, A.V. Ruban, Effect of Ni and Mn on the formation of Cu precipitates in α-Fe, Scr. Mater. 102 (2015) 11–14.
[94] S. Vaynman, D. Isheim, R.P. Kolli, S.P. Bhat, D.N. Seidman, M.E. Fine, High-strength low-carbon ferritic steel containing Cu-Fe-Ni-Al-Mn precipitates, Metall. Mater. Trans. A 39 (2008) 363–373.
[95] D. Isheim, M.S. Gagliano, M.E. Fine, D.N. Seidman, Interfacial segregation at Cu-rich precipitates in a high-strength low-carbon steel studied on a sub-nanometer scale, Acta Mater. 54 (2006) 841–849.
[96] D. Isheim, R.P. Kolli, M.E. Fine, D.N. Seidman, An atom-probe tomographic study of the temporal evolution of the nanostructure of Fe-Cu based high-strength low-carbon steels, Scr. Mater. 55 (2006) 35–40.
[97] M.K. Miller, B.D. Wirth, G.R. Odette, Precipitation in neutron-irradiated Fe-Cu and Fe-Cu-Mn model alloys: a comparison of APT and SANS data, Mater. Sci. Eng. A 353 (2003) 133–139.
[98] K. Osamura, H. Okuda, K. Asano, M. Furusaka, K. Kishida, F. Kurosawa, R. Uemori, SANS study of phase decomposition in Fe-Cu alloy with Ni and Mn addition, ISIJ Int. 34 (1994) 346–354.
[99] F. Maury, N. Lorenzelli, M.H. Mathon, C.H. de Novion, P. Lagarde, Copper precipitation in FeCu, FeCuMn, and FeCuNi dilute alloys followed by X-ray absorption spectroscopy, J. Phys. Condens. Matter 6 (1994) 569.
[100] F. Hori, A. Morita, R. Oshima, Radiation-enhanced precipitation in FeCu(C) alloys studied by electron microscopy, J. Electron Microsc. 48 (1999) 585–589.
[101] N. Maruyama, M. Sugiyama, T. Hara, H. Tamehiro, Precipitation and phase transformation of copper particles in low alloy ferritic and martensitic steels, Mater. Trans. JIM 40 (1999) 268–277.
[102] K. Osamura, H. Okuda, S. Ochiai, M. Takashima, K. Asano, M. Furusaka, K. Kishida, F. Kurosawa, Precipitation hardening in Fe-Cu binary and quaternary alloys, ISIJ Int. 34 (1994) 359–365.
[103] D. Isheim, D.N. Seidman, Nanoscale studies of segregation at coherent heterophase interfaces in α-Fe based systems, Surf. Interface Anal. 36 (2004) 569–574.